UNITED STATES DEPARTMENT OF THE INTERIOR

GEOLOGICAL SURVEY

A Numerical Study of Some Potential Sources of Error in Side-by-Side Seismometer Evaluations

by

L. Gary Holcomb

Open-File Report 90-406

This report is preliminary and has not been reviewed for conformity with U.S. Geological Survey editorial standards. Any use of trade names is for descriptive purposes only and does not imply endorsement by the U.S. Geological Survey.

Albuquerque, New Mexico

1990

Table of Contents

1 INTRODUCTION ..... 1 - 1

2 MODEL MATHEMATICAL RELATIONSHIPS ..... 2 - 1
2.1 BASIC MODEL EQUATIONS ..... 2 - 1
2.2 SOLUTION OF MODEL EQUATIONS ..... 2 - 2

3 COHERENCE ..... 3 - 1

4 DATA PROCESSING ..... 4 - 1

5 RESOLUTION LIMITS AT HIGH SIGNAL-TO-NOISE RATIOS ..... 5 - 1
5.1 WHITE SYSTEM NOISE IN WHITE BACKGROUND ..... 5 - 1
5.2 WHITE SYSTEM NOISE IN BANDSHAPED BACKGROUND ..... 5 - 6

6 MISALIGNMENT ERRORS ..... 6 - 1
6.1 WHITE BACKGROUND ..... 6 - 1
6.2 BANDSHAPED BACKGROUND ..... 6 - 9

7 QUIET SITE VERSES NOISY SITE TESTING ..... 7 - 1

8 HIGH BACKGROUND LINEARITY MEASUREMENTS ..... 8 - 1

9 CONCLUSIONS AND RECOMMENDATIONS ..... 9 - 1

10 REFERENCES ..... 10 - 1

Table of Figures

Block diagram of test configuration ..... 2 - 1
Minimum SNR's at low coherence levels ..... 3 - 2
Minimum SNR's at high coherence levels ..... 3 - 2
PSD estimates - white noise in white background SNR 1 ..... 5 - 3
PSD estimates - white noise in white background SNR 10 ..... 5 - 3
PSD estimates - white noise in white background SNR 100 ..... 5 - 4
PSD estimates - white noise in white background SNR 1000 ..... 5 - 4
PSD estimates - white noise in white background SNR 10000 ..... 5 - 5
PSD estimates - white noise in white background SNR 100000 ..... 5 - 5
Bandstop filter amplitude response ..... 5 - 7
PSD estimates - white noise in shaped background SNR 1 ..... 5 - 8
PSD estimates - white noise in shaped background SNR 10 ..... 5 - 8
PSD estimates - white noise in shaped background SNR 100 ..... 5 - 9
PSD estimates - white noise in shaped background SNR 1000 ..... 5 - 9
PSD estimates - white noise in shaped background SNR 10000 ..... 5 - 10
PSD estimates - white noise in shaped background SNR 100000 ..... 5 - 10
PSD estimates - white background at 0.1 degree misalignment ..... 6 - 3
PSD estimates - white background at 0.1 degree misalignment ..... 6 - 3
PSD estimates - white background at 2.0 degree misalignment ..... 6 - 4
PSD estimates - white background at 3.0 degree misalignment ..... 6 - 4
PSD estimates - white background at 4.0 degree misalignment ..... 6 - 5
PSD estimates - white background at 5.0 degree misalignment ..... 6 - 5
White noise maximum detectable SNR vs misalignment ..... 6 - 6
White noise maximum detectable SNR vs misalignment ..... 6 - 6
White noise maximum detectable SNR vs misalignment ..... 6 - 7
White noise coherence as function of misalignment ..... 6 - 7
White noise coherence as function of misalignment ..... 6 - 8
White noise coherence as function of misalignment ..... 6 - 8
White noise 1-GAMMA**2 as function of misalignment ..... 6 - 8
PSD estimate - bandshaped background 0.1 degree misalignment ..... 6 - 11
PSD estimates - bandshaped background 1 degree misalignment ..... 6 - 11
PSD estimates - bandshaped background 2 degree misalignment ..... 6 - 12
PSD estimates - bandshaped background 3 degree misalignment ..... 6 - 12
PSD estimates - bandshaped background 4 degree misalignment ..... 6 - 13
PSD estimates - bandshaped background 5 degree misalignment ..... 6 - 13
Bandshaped maximum detectable SNR vs misalignment ..... 6 - 15
Bandshaped maximum detectable SNR vs period ..... 6 - 15
Bandshaped noise coherence as function of misalignment ..... 6 - 16

1 INTRODUCTION

This report presents the results of a series of computer simulations of potential errors in test data, which might be obtained when conducting side-by-side comparisons of seismometers. These results can be used as guides in estimating potential sources and magnitudes of errors one might expect when analyzing real test data.

First, the derivation of a direct method for calculating the noise levels of two sensors in a side-by-side evaluation is repeated and extended slightly herein. This bulk of this derivation was presented previously (see Holcomb 1989); it is repeated here for easy reference.

This method is applied to the analysis of a simulated test of two sensors in a side-by-side test in which the outputs of both sensors consist of white noise spectra with known signal-to-noise ratios (SNR's). This report extends this analysis to high SNR's to determine the limitations of the direct method for calculating the noise levels at signal-to-noise levels which are much higher than presented previously (see Holcomb 1989).

Next, the method is used to analyze a simulated test of two sensors in a side-by-side test in which the outputs of both sensors consist of bandshaped noise spectra with known signal-to-noise ratios. This is a much more realistic representation of real world data because the earth's background spectrum is certainly not flat.

Finally, the results of the analysis of simulated white and bandshaped side-by-side test data are used to assist in interpreting the analysis of the effects of simulated azimuthal misalignment in side-by-side sensor evaluations. A thorough understanding of azimuthal misalignment errors is important because of the physical impossibility of perfectly aligning two sensors in a real world situation. The analysis herein indicates that alignment errors place lower limits on the levels of system noise which can be resolved in a side-by-side measurement. It also indicates that alignment errors are the source of the fact that real data noise spectra tend to follow the earth's background spectra in shape.

2 MODEL MATHEMATICAL RELATIONSHIPS

The system to be evaluated is modeled in Figure 2.1 where X is assumed to be the coherent ground motion power spectral density (PSD) input to both systems. All quantities in the figure are assumed to be functions of frequency. Experimentally, the observer does not know X, N_1, and N_2; the signals appearing at ports 1 and 2 are the only two time functions whose PSD functions (P_{11} and P_{22}) are available for measurement and analysis. In addition, the system transfer functions (H_1 and H_2) are assumed to be known. The circle containing "S" denotes a summing junction.

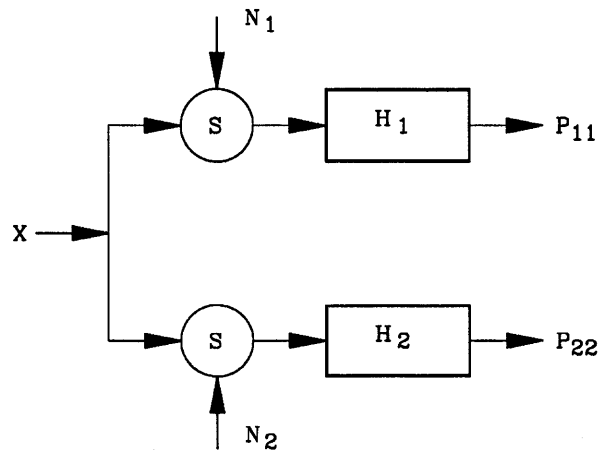

Figure 2.1 Linear system model of side-by-side evaluation of two seismometer systems.

2.1 BASIC MODEL EQUATIONS

Figure 2.1 contains a block diagram depicting the configuration of two seismometer systems operating in close enough proximity to one another that the seismic signal input power X may be assumed to be at the same level and coherent between the sensors. The two systems are assumed to have system transfer functions H_1 and H_2 which are not necessarily equal. In addition the sensors are assumed to be generating incoherent self noise powers N_1 and N_2 referred to the input, not necessarily equal.

The relationships between power at various points in the block diagram in Figure 2.1 can be written in terms of system equations which relate the power outputs from the systems to the power appearing at the inputs of the systems. The power spectral density of the output of system 1 is given by

$$P_{11} = |H_1|^2 [X + N_1] \qquad \textit{Equation} \quad 2.1$$

and the same quantity for system 2 is

$$P_{22} = |H_2|^2 [X + N_2] \qquad \textit{Equation} \quad 2.2$$

The cross spectral density between the outputs of the two systems may be written as

$$P_{12} = H_1 H_2^* X \qquad \textit{Equation} \quad 2.3$$

2.2 SOLUTION OF MODEL EQUATIONS

The solution of these three equations depends on the desired information one needs to acquire. In the case of test and evaluation of two seismometers operating side-by-side, one frequently needs estimates of the noise levels associated with the subject instruments. This information can easily be obtained directly from the three equations without resorting to intermediate definitions of additional quantities such as the coherence function or the SNR as follows. Simply solve Equation 2.1 for N_1 to yield

$$N_1 = \frac{P_{11}}{|H_1|^2} - X \qquad \textit{Equation} \quad 2.4$$

Substituting for X from Equation 2.3 yields

$$N_1 = \frac{P_{11}}{|H_1|^2} - \frac{P_{12}}{H_1 H_2^*} \qquad \textit{Equation} \quad 2.5$$

Similarly, solving Equation 2.2 for N_2 and substituting for X from Equation 2.3 yields

$$N_2 = \frac{P_{22}}{|H_2|^2} - \frac{P_{12}}{H_1 H_2^*} \qquad \textit{Equation} \quad 2.6$$

The two system noise power spectra in Equations 2.5 and 2.6 are expressed in terms of directly measurable quantities at the outputs of the two test systems and the system transfer functions. It is important to observe that both noise estimates are evaluated independently from one another. This means that it is possible to directly obtain noise estimates from two sensors whose noise characteristics are significantly different from one another.

3 COHERENCE

Since the system noise spectra can be derived directly, as has been demonstrated above, the question arises as to the utility of the coherence function. The coherence function can be used to make preliminary estimates of the systems SNR's and to place lower limits on the SNR's as will now be shown.

The coherence function is defined as (see Bendat and Piersol, 1971 p 32)

$$\gamma^2 = \frac{|P_{12}|^2}{P_{11}P_{22}} \qquad \textit{Equation} \quad 3.1$$

Substituting for P_{11}, P_{22}, and P_{12} from equations 2.1, 2.2, and 2.3 respectively yields

$$\gamma^2 = \frac{|H_1 H_2^* X|^2}{|H_1|^2 [X + N_1] \, |H_2|^2 [X + N_2]} \qquad \textit{Equation} \quad 3.2$$

The response functions divide out of the expression leaving

$$\gamma^2 = \frac{X^2}{X^2 + X(N_1 + N_2) + N_1 N_2} \qquad \textit{Equation} \quad 3.3$$

Inverting, multiplying both sides by X^2, and dividing both sides by N_1N_2 yields

$$\frac{1}{\gamma^2}\frac{X^2}{N_1N_2} = \frac{X^2}{N_1N_2} + \frac{X}{N_2} + \frac{X}{N_1} + 1 \qquad \textit{Equation} \quad 3.4$$

Rearranging we have

$$\frac{X}{N_1}\frac{X}{N_2}\left(1 - \frac{1}{\gamma^2}\right) + \frac{X}{N_1} + \frac{X}{N_2} + 1 = 0 \qquad \textit{Equation} \quad 3.5$$

This expression relates the power SNR's of the two channels to the coherence and it is in the form of the general equation of an equilateral hyperbola. Figure 3.1 presents the interrelationship of the two channel SNR's for 9 values of coherence spaced 0.1 apart and Figure 3.2 extends the plot to high values of coherence extending from 0.90 to 0.99.

The asymptotes to these hyperbolas are given by

$$\frac{X}{N_1} = \frac{X}{N_2} = \frac{\gamma^2}{1 - \gamma^2} \qquad \textit{Equation} \quad 3.6$$

Therefore, given a value of the coherence between the output signals of a side-by-side test of two instruments, the power SNR's in both instruments must be at least as high as the value given by Equation 3.6. Since it is unlikely that, under low background conditions, the SNR on one instrument will greatly exceed that in the other if the PSD's are somewhat equal, the plots in Figures 3.1 and 3.2 can be used to obtain quick estimates of the system SNR's.

The special case of equal SNR's in both channels can be analyzed by letting $N_1 = N_2$ ($\frac{X}{N_2} = \frac{X}{N_2}$) in Equation 3.5 and solving for the quadratic for the SNR. The root is found to be

$$\frac{X}{N_1} = \frac{X}{N_2} = \frac{\gamma}{1-\gamma} \qquad \textit{Equation} \quad 3.7$$

This condition is the special case of equal noise in both sensors which was modeled at ASL earlier (see Peterson *et al.* 1980).

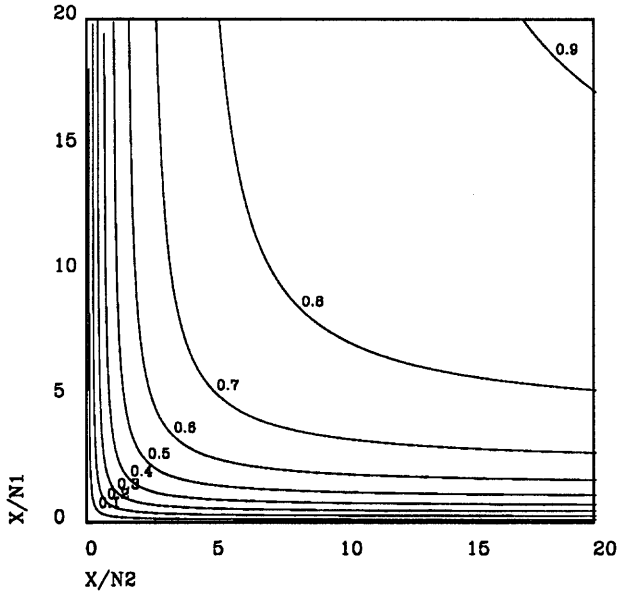

Figure 3.1 The interrelationship of the channel power SNR's and coherence at low levels of coherence.

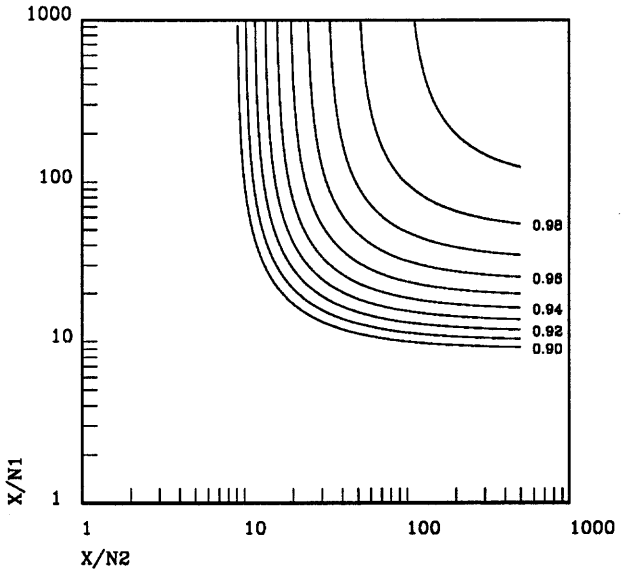

Figure 3.2 The interrelationship of the channel power SNR's and coherence at high levels of coherence.

Equation 3.6 can be solved for $N_1 = N_2 = N$ to yield

$$N = X\left(\frac{1}{\gamma^2} - 1\right) \qquad \textit{Equation} \quad 3.8$$

and substituting for X from equation 2.3

$$N = \frac{P_{12}}{H_1 H_2^*}\left(\frac{1}{\gamma^2} - 1\right) \qquad \textit{Equation} \quad 3.9$$

Equation 3.9 can be used to calculate absolute upper limits based on the coherence (the asymptotic limits) for the noise in both sensors involved in a test. The noise estimates calculated from equations 3.5 and 3.6 should both lie below that indicated by equation 3.9 throughout the sensor passband.

4 DATA PROCESSING

All time series data processed in this report were composed of dummy data that was generated in the computer with a random number generator (see Stearns & David 1988, pp 52-54). The time series were uniformly distributed with well known white PSD levels.

The linear system model contained in Figure 2.1 was assumed to be an accurate model for the test configurations analyzed in this report. Incoherent, internally generated time series representing X, N_1, and N_2 were added as shown in Figure 2.1. Their sums were then digitally filtered with a lowpass Butterworth antialias filter with a cutoff of 4 seconds and an attenuation 40 db down at 3 seconds (see Stearns & David 1988, pp 153-156). The time series were then decimated by a factor of two, divided into segments 2048 points long, and a 50% overlap between segments was generated.

The system transfer functions for both channels 1 and 2 (H_1 and H_2) respectively in Figure 2.1) were assumed to be flat with an amplitude of 1 and zero phase shift.

Prior to calculating the Fast Fourier Transform (FFT), each segment was windowed using a Hanning window. The FFT of each segment was calculated using the FFT algorithm from Stearns, 1975, p 265. Total system output power levels (P_{11} and P_{22} in Figure 2.1) were evaluated by calculating the power contained in the FFT's of their respective output time series. The cross spectral density (CPSD) between the two channels (P_{12} in Figure 2.1) was evaluated by calculating the amplitude of the cross spectral power between the two output FFT's (see Bendat & Piersol, 1971 p 333).

The PSD estimates were smoothed using a combination of ensemble averaging and frequency smoothing (see Bendat & Piersol pp. 329-330). A total of 39 data segments were averaged to produce each of the PSD estimates. The frequency smoothing algorithm, which is used to smooth in the frequency domain, was the one developed earlier by the author (see Holcomb, 1989, pp. 6-2 - 6-5).

Equations 2.5 and 2.6 were used to calculate the direct model noise PSD estimates (N_1 and N_2) and Equation 3.9 was used to calculate the coherence derived asymptotic upper limits for the noise levels (N).

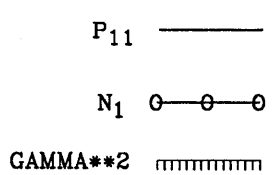

Figure 4.1 Line definition for the PSD plots contained in this report.

Figure 4.1 contains a definition of the data represented by the three types of lines plotted in each PSD plot contained in this report. The plain line depicted as P_{11} in Figure 4.1 represents the total output PSD calculated for channel 1. Since both channels are equally noisy in the examples contained in this report, this line also represents the total output PSD for channel 2. The line depicted as N_1 with O's superimposed on it in Figure 4.1 represents the noise PSD estimate as calculated from Equation 2.5 for channel 1. It is also an estimate of the noise level for channel 2 because both channels are equally noisy. The line depicted as GAMMA**2 with hatch marks below it in Figure 4.1 represents the asymptotic maximum noise level (N) for both sensors as calculated from the coherence function using equation 3.9.

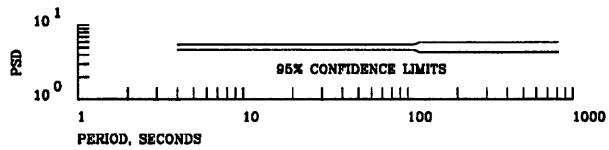

Figure 4.2 Confidence intervals for all PSD plots in this report.

Figure 4.2 contains a plot of the 95% confidence intervals for the data in the PSD plots. Note that the confidence interval is not a constant at all periods as is customarily the case. Instead, it increases as the period increases. This increase is due to the unique frequency smoothing which was used to smooth the PSD data.

5 RESOLUTION LIMITS AT HIGH SIGNAL-TO-NOISE RATIOS

It is important that the limits of validity of the direct model be known when applying the model to analyze real test data. A question which naturally arises is how low a level of incoherent noise can be resolved in a given level of coherent signal. Two different conditions were modeled and analyzed for this study. The first condition contained white noise in a white signal; the second contained white noise in a bandshaped signal.

5.1 WHITE SYSTEM NOISE IN WHITE BACKGROUND

A random number generator (see Stearns & David 1988, pp 52-54) was used to create uncorrelated time sequences to represent N_1, N_2, and X whose power spectral density levels were accurately known. For simplicity, the response functions of both simulated sensors were assumed to be flat with zero phase shift. The relative normalized levels of the respective input PSD's are shown in the linear system model portion of the PSD plots contained in this section.

The results of analyzing imaginary sensors whose SNR's range from 1 to 100000 are presented in Figures 5.1 through 5.6. The coherent PSD input to each simulated sensor system was kept constant throughout all five simulated conditions; the incoherent noise level was varied to achieve the indicated SNR. The analysis of this data follows the procedures outlined in the earlier report (see Holcomb 1989); in particular, the smoothing operation outlined there was used to process all of the data contained in this report.

At first glance, the data contained in Figure 5.1 may seem in error because it may seem strange that the asymptotic coherence PSD estimate for the sensor noise levels derived from equation 3.9 lies above the total power PSD estimate for each channel. This is a physical impossibility but the mathematics is correct as follows. Both channels in Figure 5.1 are equally noisy with SNR's of 1; therefore, from Equation 3.7, γ is equal to 0.5. Equation 3.8 indicates that $N = 3X$ for $\gamma^2 = 0.25$. The coherent power in Figure 5.1 lies at 10^{-12}; therefore, the asymptotic coherence noise PSD lies at 3×10^{-12} just as it is plotted, where as, the total noise power is 2×10^{-12} as shown. Hence, this is an example of how much a γ^2 estimate of system noise power can be in error; in this case it is three times the actual noise power.

The direct method calculated noise levels are very accurate at SNR's of 0.5 and 10 in Figures 5.1 and 5.2. At SNR's of 100 and 1000 in Figures 5.3 and 5.4, the direct method noise estimates are quite good from 4 to 100 seconds. Above 100 seconds, the estimated noise levels are slightly higher than they should be but they are not too far off. This is probably due to the increase in the confidence intervals above 100 seconds. At SNR's of 10000 and 100000 in Figures 5.5 and 5.6, the direct method noise estimates are progressively higher than the known levels. The increasing error at higher SNR's is probably due to statistical errors in estimating the two output PSD's and the cross spectral density function.

In contrast, the asymptotic coherence derived maximum noise level estimates for SNR's of 1 and 10 in Figures 5.1 and 5.2 are significantly higher than the known levels (3x and approximately 2x respectively). As γ^2 gets large, the asymptotic coherence derived maximum noise level becomes twice as large as the actual noise level. This is observable in Figures 5.1 through

5.6 or provable by taking the ratio of Equation 3.6 (the asymptotic SNR) to Equation 3.7 (the actual SNR if the channels are equally noisy). Note that the asymptotic coherence derived maximum noise levels at SNR's of 100 and 1000 in Figures 5.3 and 5.4 are nearly as accurate as the direct model derived estimates of the noise levels particularly at periods of 100 seconds and beyond. At SNR's of 10000 and 100000 in Figures 5.5 and 5.6, the asymptotic coherence derived maximum noise level is closer to the known noise level than are the direct model estimates.

The conclusion to be drawn from this set of data is that the direct method produces better results at low SNR's whereas the asymptotic coherence derived maximum noise level estimate is more accurate at very high SNR's. In real world seismic sensors it is unlikely that extremely high SNR's will be encountered if tests are conducted under quiet background conditions. Therefore, the direct method of processing the test data should yield the most reliable results. However, it may be desirable to evaluate both the direct method derived estimate and the asymptotic coherence derived maximum noise level estimate as has been done in Figures 5.1 through 5.6 to see if indeed the direct estimate is the smallest. If not, the indication is that the direct estimate is in error and that the asymptotic estimate is closer to the true value.

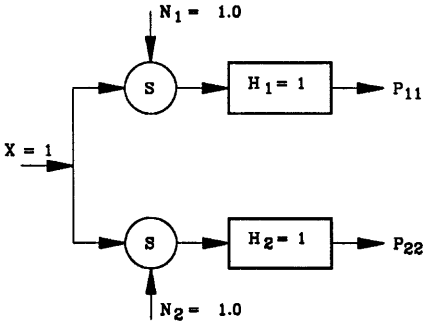

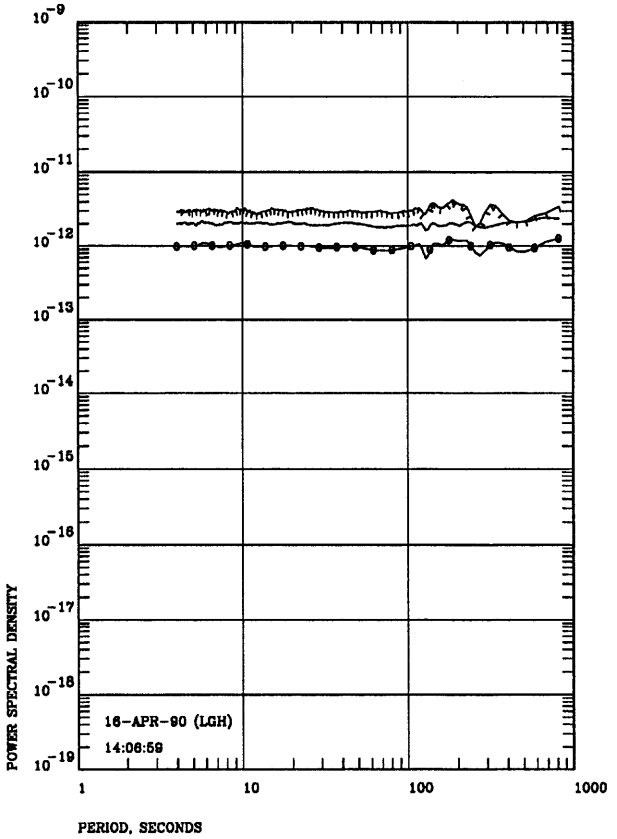

Figure 5.1 Linear system model and PSD estimates for white noise in a white background spectra with a SNR of 1. The known noise PSD lies at 10^{-12}. See Figure 4.1 for line definition.

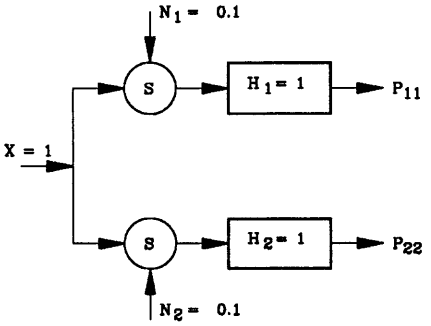

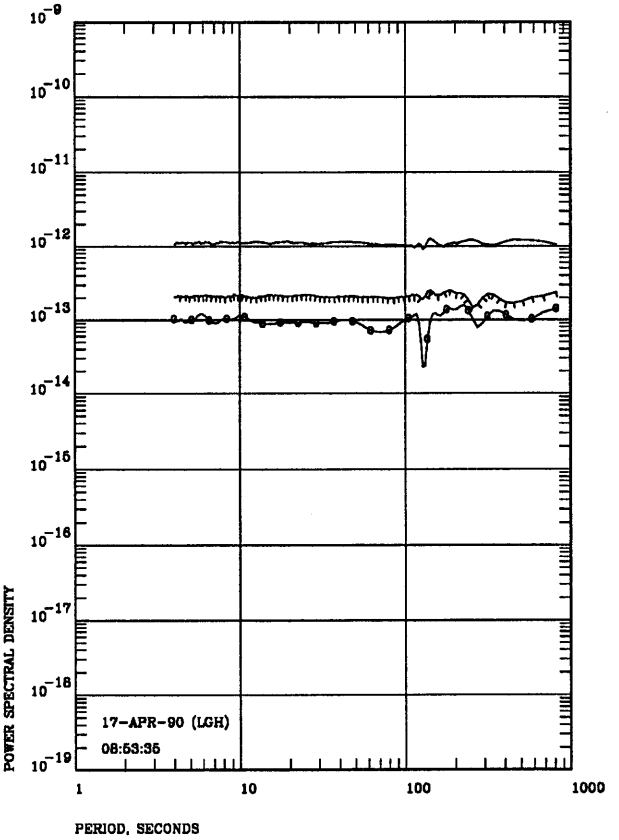

Figure 5.2 Linear system model and PSD estimates for white noise in a white background spectra with a SNR of 10. The known noise PSD lies at 10^{-13}. See Figure 4.1 for line definition.

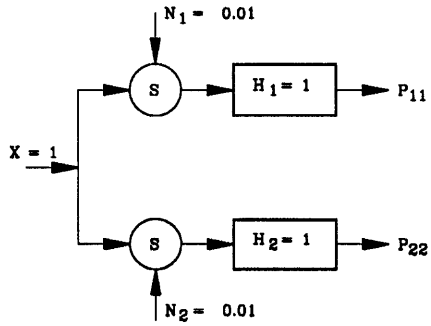

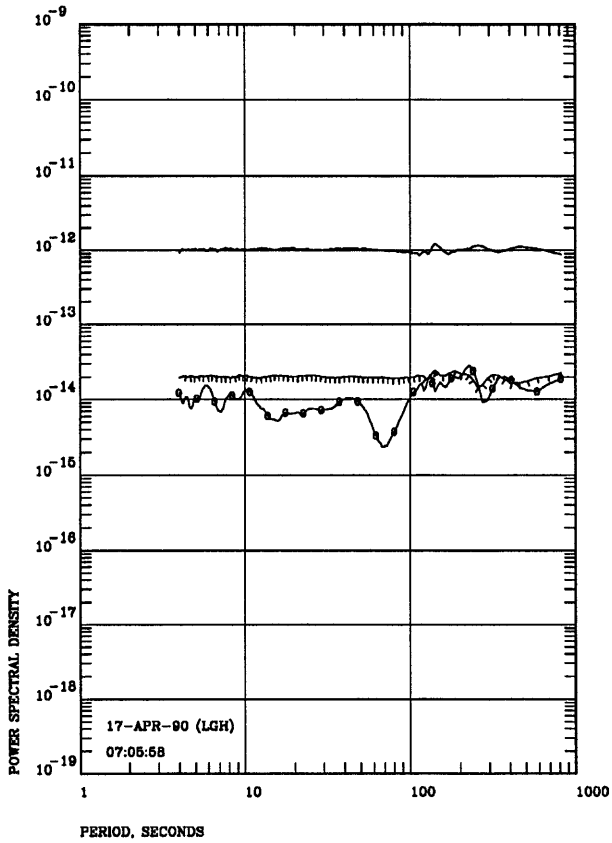

Figure 5.3 Linear system model and PSD estimates for white noise in a white background spectra with a SNR of 100. The known noise PSD lies at 10^{-14}. See Figure 4.1 for line definition.

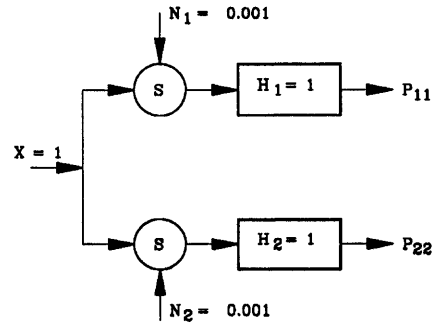

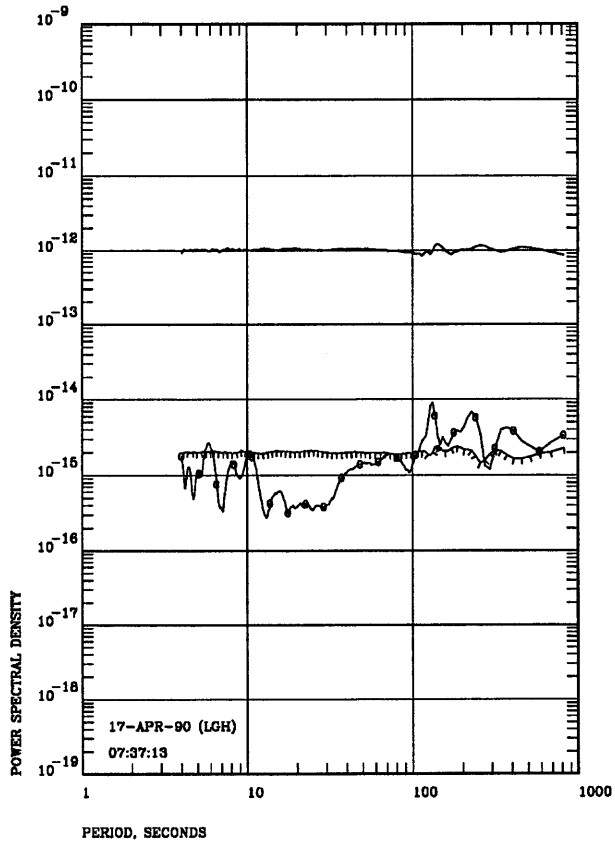

Figure 5.4 Linear system model and PSD estimates for white noise in a white background spectra with a SNR of 1000. The known noise PSD lies at 10^{-15}. See Figure 4.1 for line definition.

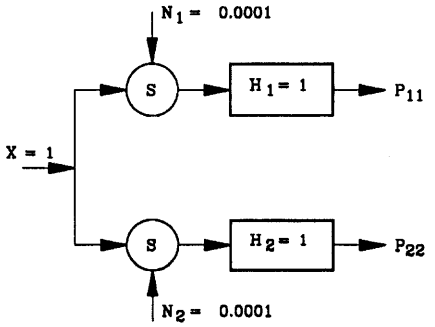

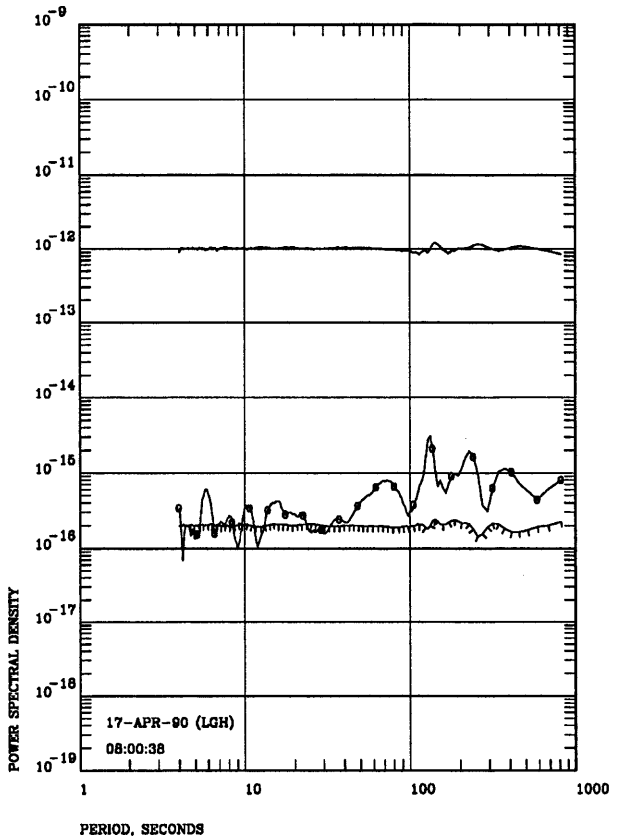

Figure 5.5 Linear system model and PSD estimates for white noise in a white background spectra with a SNR of 10000. The known noise PSD lies at 10^{-16}. See Figure 4.1 for line definition.

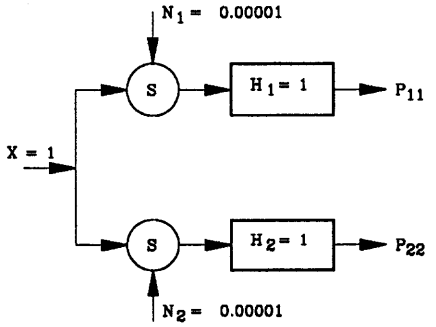

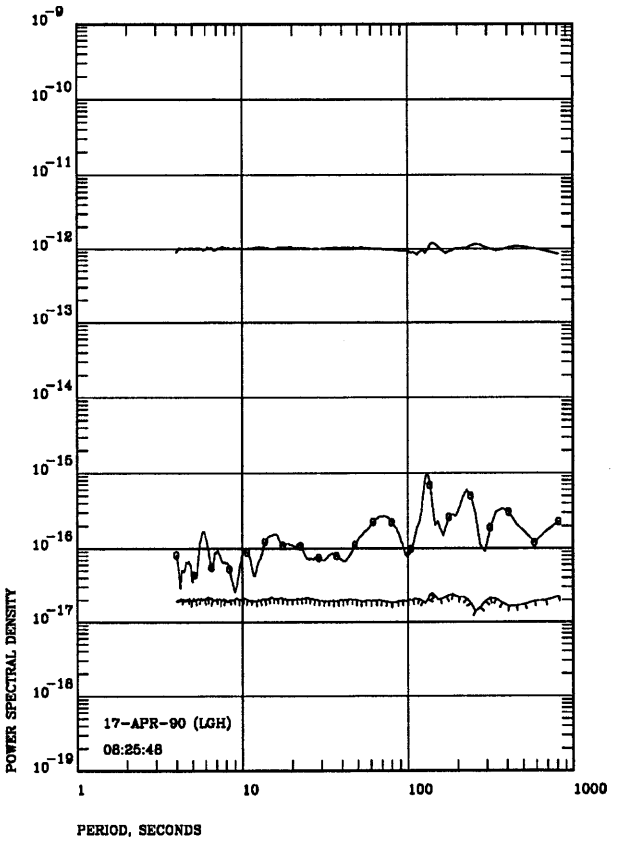

Figure 5.6 Linear system model and PSD estimates for white noise in a white background spectra with a SNR of 100000. The known noise PSD lies at 10^{-17}. See Figure 4.1 for line definition.

5.2 WHITE SYSTEM NOISE IN BANDSHAPED BACKGROUND

Bandshaped artificial background noise was created by bandstop filtering the white coherent input time series (see the linear system model in Figure 5.8 for example). A Chebyshev type II bandstop filter was used with an amplitude response as depicted in Figure 5.7 (see Stearns & David, pp 153-156). This response had been determined by trial and error to produce an output power spectrum which somewhat approximated a quiet site background acceleration spectrum.

The input power level to the filter was held constant, as it was in the white background noise study in Section 5.1 above, and the white incoherent noise levels were varied over the same range as above to create the same out of band (by out of band the author means that portion of the spectrum not attenuated by the band stop filter) SNR's as above.

Figures 5.8 through 5.13 contain the results of analyzing this simulation of earth background shaped coherent input data. The known levels of artificial system noise are denoted in the captions of each figure and the normalized levels of noise added are given in the linear system model at the top of the figures. Note that the total output PSD of Figure 5.13 is a fair approximation to a quiet site background acceleration spectra.

In general, the noise estimates calculated by the direct method agree quite well with the known level of the system noise in all 6 cases. The estimates below about 20 seconds in Figures 5.12 and 5.13 are slightly higher than they should be; this error probably corresponds to the saturation of the direct processing at high SNR's as was seen in the white noise study of Section 5.1.

The performance of the asymptotic coherence determined maximum noise level estimate is considerably worse particularly when the SNR is very low. This is true in the stop band portion of the spectrum (from about 20 to 700 seconds) at relatively high noise levels (see Figures 5.8 through 5.11) where the asymptotic upper limit estimated PSD levels are considerably above the known level. This error is due to the failure of the cross spectral density function to resolve coherent power at low SNR's. The CPSD estimates are too high in the stop band portion of the spectrum thus leading to asymptotic coherence determined maximum noise level estimates which are too high.

Two important points can be drawn from this portion of the study. First, the direct method is capable of resolving sensor noise levels in the presence of bandshaped background over a fairly broad range of SNR's. Second, the calculated noise spectra do not necessarily follow the shape of the background spectra.

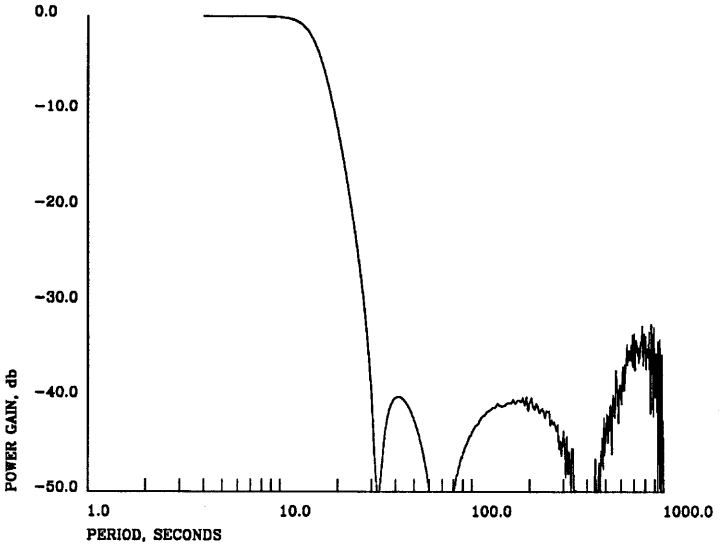

Figure 5.7 Amplitude response of digital bandstop filter used to reshape white noise into a spectra resembling the earth's background spectral shape.

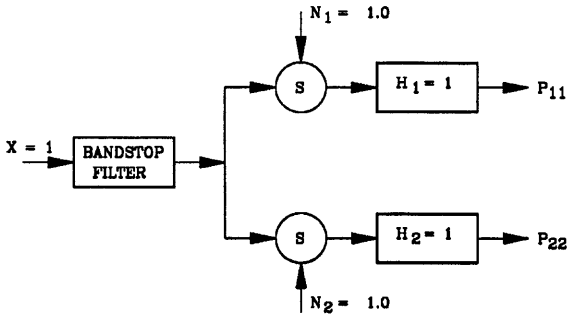

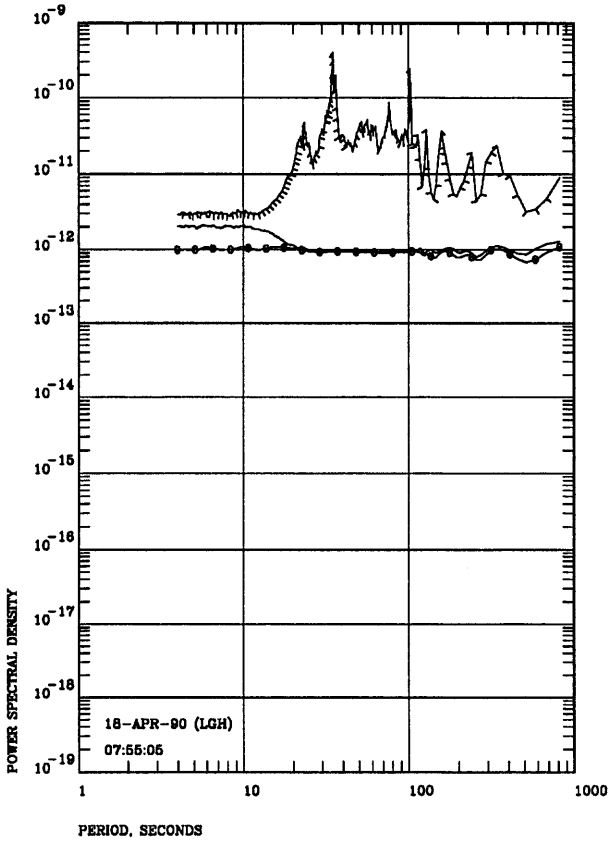

Figure 5.8 Linear system model and PSD estimates for white noise in a bandshaped background spectra with an out of band SNR of 1. The known noise PSD lies at 10^{-12}. See Figure 4.1 for line definition.

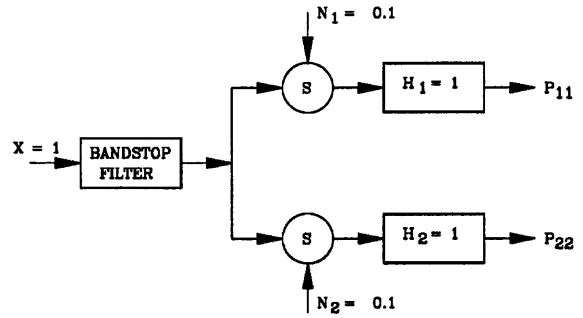

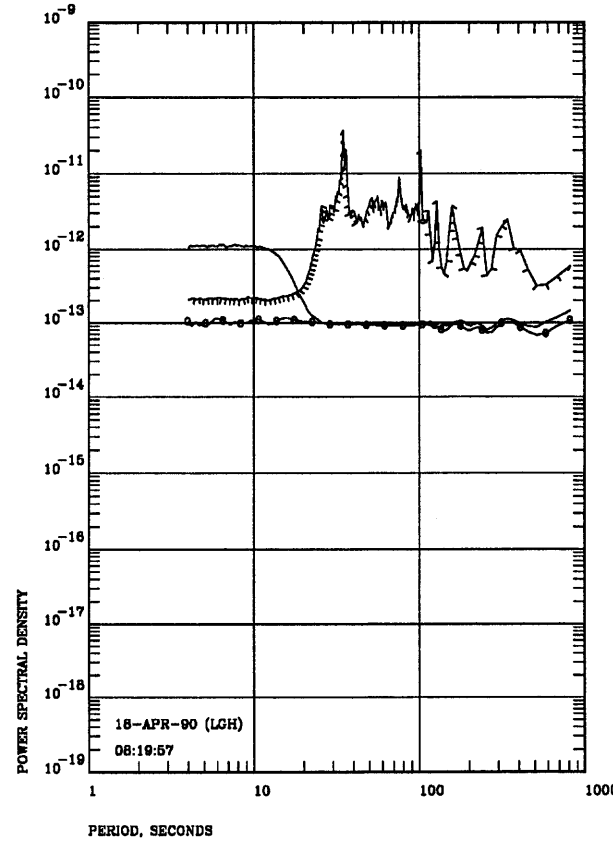

Figure 5.9 Linear system model and PSD estimates for white noise in a bandshaped background spectra with an out of band SNR of 10. The known noise PSD lies at 10^{-13}. See Figure 4.1 for line definition.

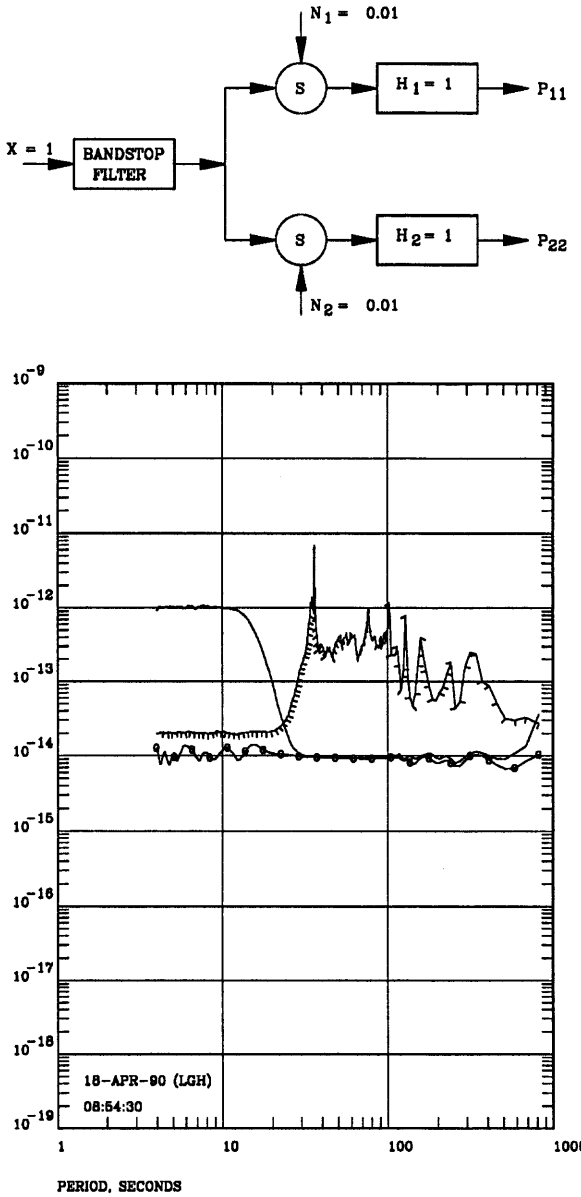

Figure 5.10 Linear system model and PSD estimates for white noise in a bandshaped background spectra with an out of band SNR of 100. The known noise PSD lies at 10^{-14}. See Figure 4.1 for line definition.

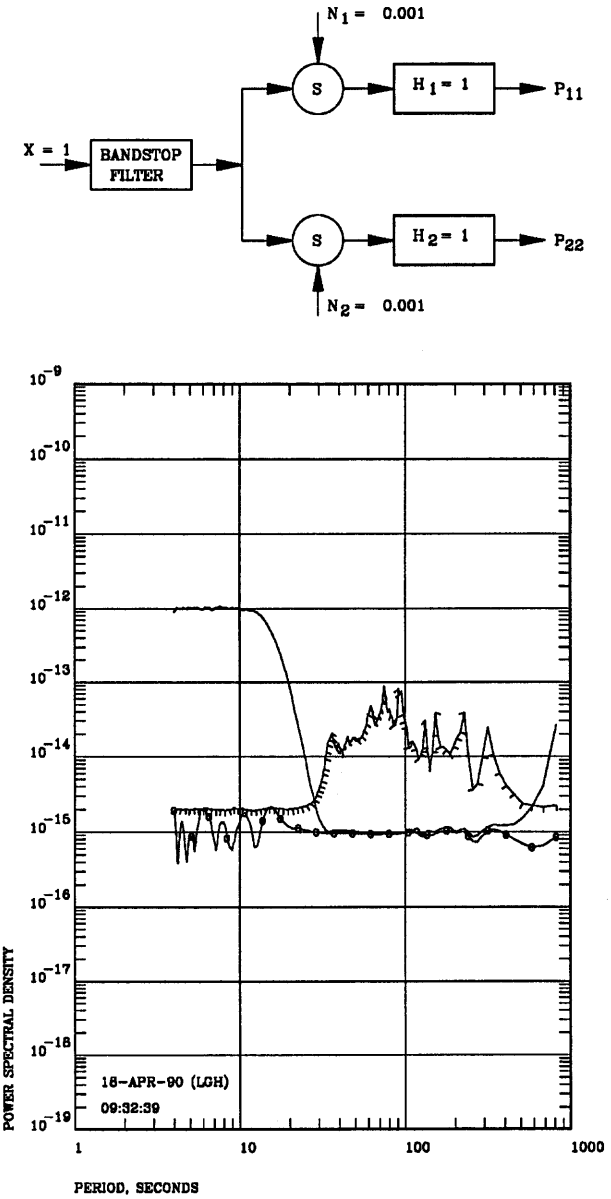

Figure 5.11 Linear system model and PSD estimates for white noise in a bandshaped background spectra with an out of band SNR of 1000. The known noise PSD lies at 10^{-15}. See Figure 4.1 for line definition.

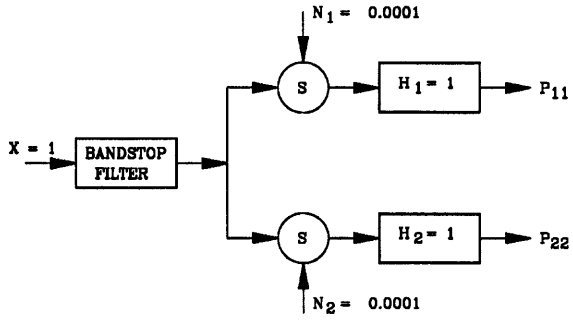

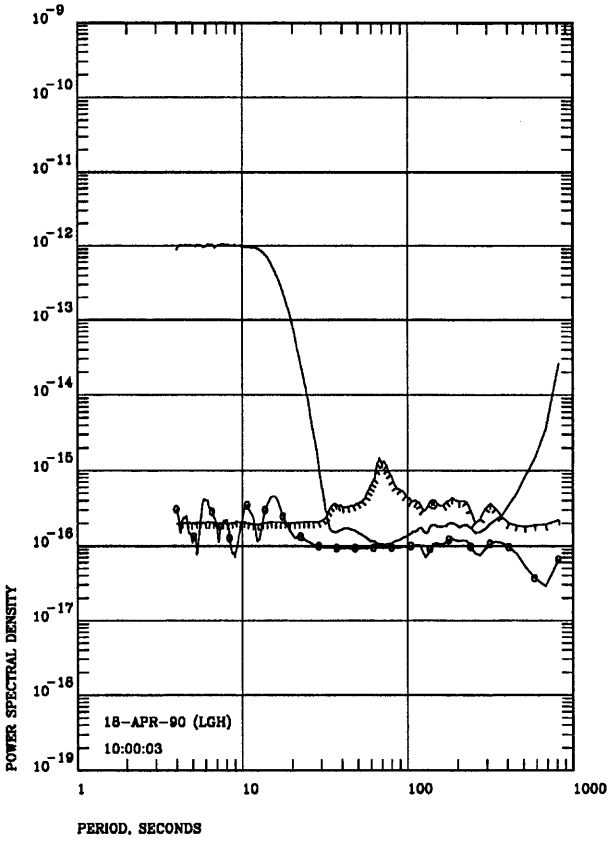

Figure 5.12 Linear system model and PSD estimates for white noise in a bandshaped background spectra with an out of band SNR of 10000. The known noise PSD lies at 10^{-16}. See Figure 4.1 for line definition.

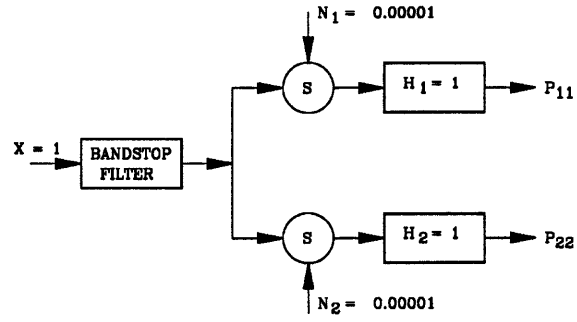

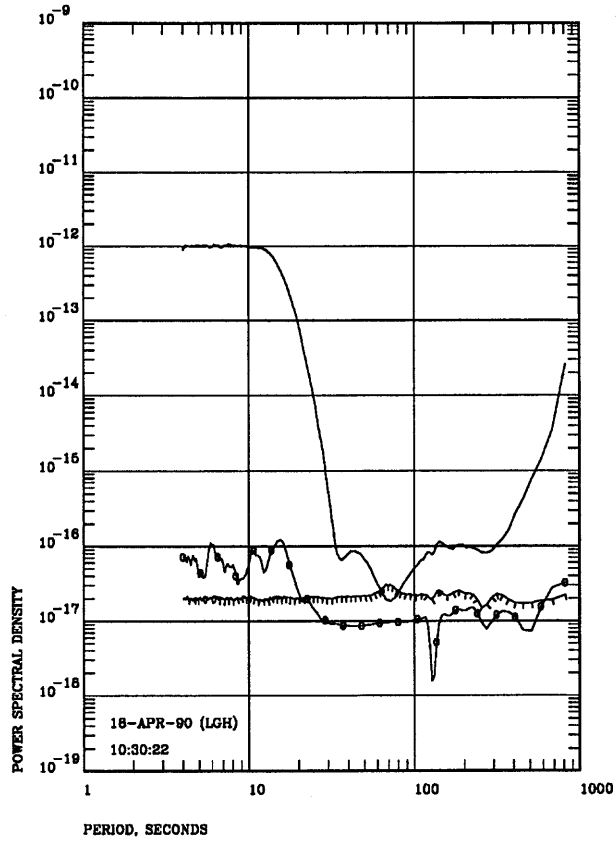

Figure 5.13 Linear system model and PSD estimates for white noise in a bandshaped background spectra with an out of band SNR of 100000. The known noise PSD lies at 10^{-17}. See Figure 4.1 for line definition.

6 MISALIGNMENT ERRORS

All of the models analyzed to this point assume that the two seismic sensors are perfectly aligned in one direction; this assures that the input signal (X) is a purely coherent signal. However, in the real world evaluation situation, it is physically impossible to repeatedly align two instruments perfectly. There will always be some degree of unknown misalignment and it is important to understand the potential effects of this type of error on the data analysis process.

In this study, the effects of instrument misalignment were investigated by rotating the input to one of the instruments in a simulated earth background composed of two orthogonal uncorrelated white time sequences, which represented orthogonal earth background input. The linear system models in the upper parts of Figures 6.1 through 6.6 are attempts to graphically depict the analysis process. In these figures, X, X_1, and X_2 represent the simulated orthogonal earth background inputs to the two sensors. For this analysis, the sensors were assumed to be ideal noise free instruments. The input to channel two was rotated in the frequency domain (see Bath, 1974 pp 229-230)

$$F_2' = X\cos\theta + X_2\sin\theta \qquad \textit{Equation} \quad 6.1$$

where F_2' is the rotated Fast Fourier Transform for the second channel and θ is the angle of misalignment of one sensor with respect to the other. The sensor in channel one was assumed to be perfectly aligned; its input consisted only of X. Therefore, $X_1 = 0$ in the linear system models in the figures.

6.1 WHITE BACKGROUND

The effects of sensor misalignment in a simulated earth background with a white PSD was investigated first. X and X_2 in the linear system models of Figures 6.1 through 6.6 were both white noise sources. The effects of misalignment angles of 0.0001, 0.001, 0.01, 0.1, 1, 2, 3, 4, 5, 10, 20 30, 40, and 50 degrees were evaluated. Figures 6.1 through 6.6 contain linear system models and the PSD estimates generated from the more practical misalignment angles of 0.1, 1, 2, 3, 4, and 5 degrees.

Figure 6.1 contains the results of the analysis of a simulated misalignment of 0.1 degrees. Note that even though the sensors themselves were assumed to be ideal noise free sensors, the misalignment creates the illusion that the channel one system noise level is at least 10^{-18} and probably higher. Note that the direct method PSD estimate lies considerably above the asymptotic coherence derived upper limit for the system noise; this is probably due to the saturation effect demonstrated by the direct method PSD estimates of high SNR white noise shown in Section 5.1. Although not shown, the results of the analysis for channel two are very similar to those for channel one. The appearance of noise due to sensor misalignment limits the resolution capability of the analysis process to calculate the noise levels in real sensors.

As the misalignment angle increases (see Figures 6.2 through 6.6) the level of the PSD estimates derived purely from alignment errors also increases to quite high levels. Figure 6.6 contains data for a five degree alignment error; a five degree error does not seem to be impractically large particularly if one considers the analysis of data from two horizontal sensors deployed in two boreholes. The alignment induced noise floor in Figure 6.6 indicates that the analysis of data from two sensors with an unknown 5 degree misalignment would be limited to resolving sensor noise with an approximate power SNR of between 100 and 1000 (assuming that the total PSD level of 10^{-12} is mostly signal).

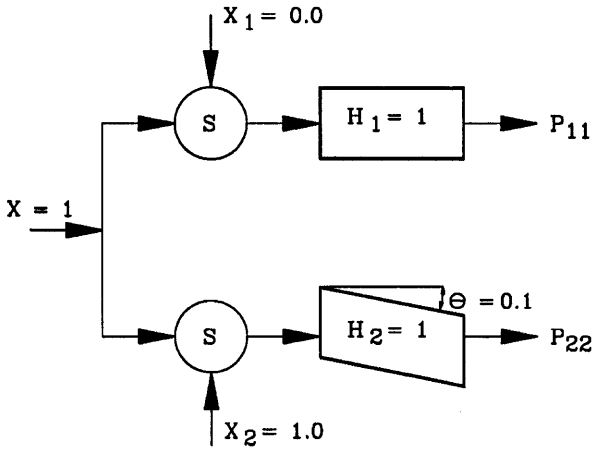

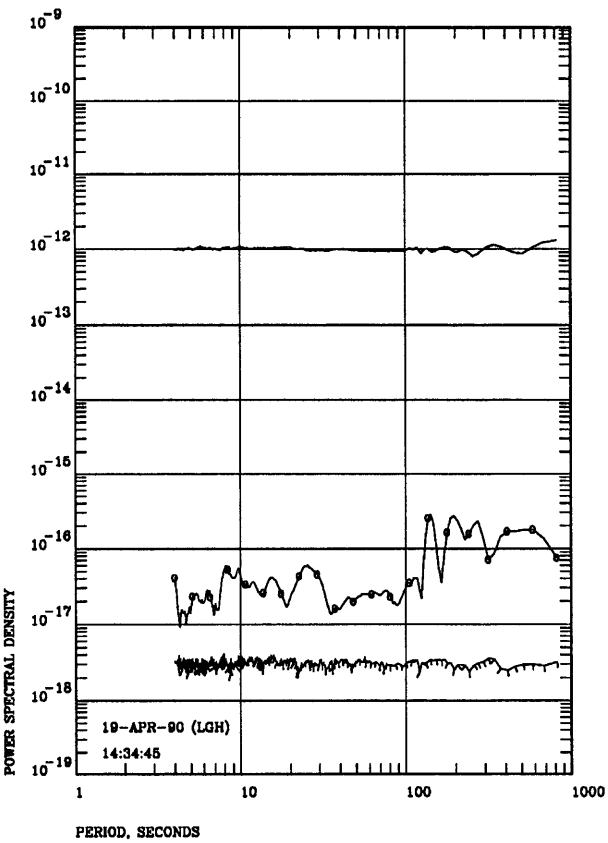

Figure 6.1 Linear system model and PSD estimates for a 0.1 degree misalignment of two sensors in a white noise environment. See Figure 4.1 for line definition.

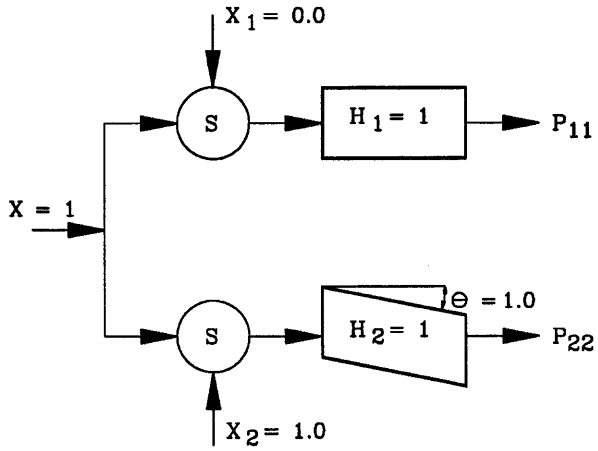

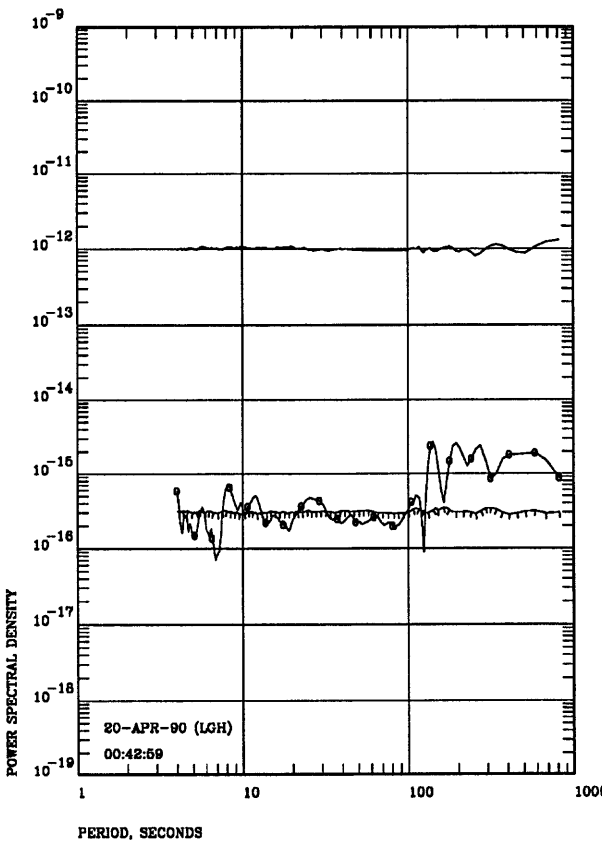

Figure 6.2 Linear system model and PSD estimates for a 1.0 degree misalignment of two sensors in a white noise environment. See Figure 4.1 for line definition.

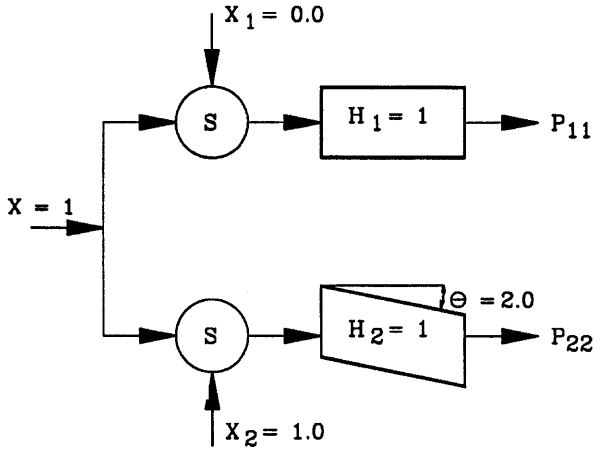

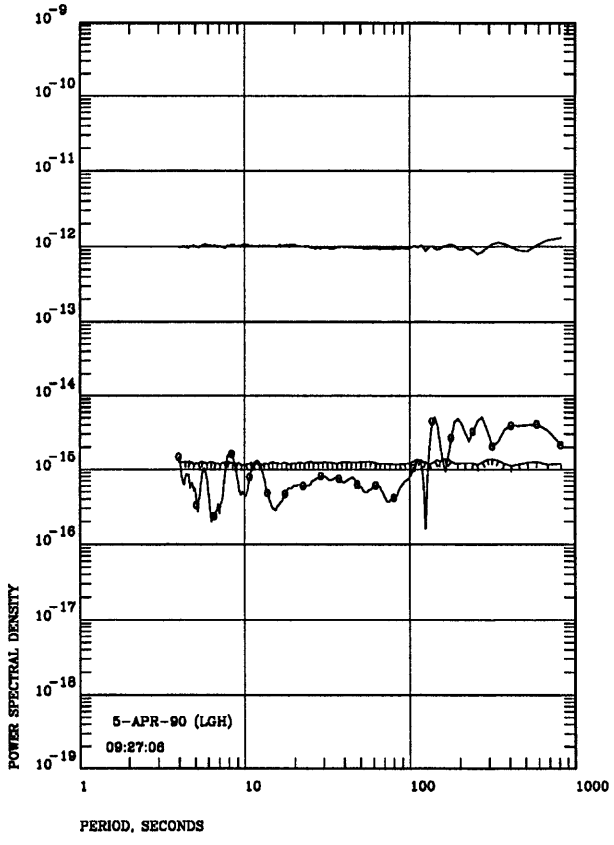

Figure 6.3 Linear system model and PSD estimates for a 2.0 degree misalignment of two sensors in a white noise environment. See Figure 4.1 for line definition.

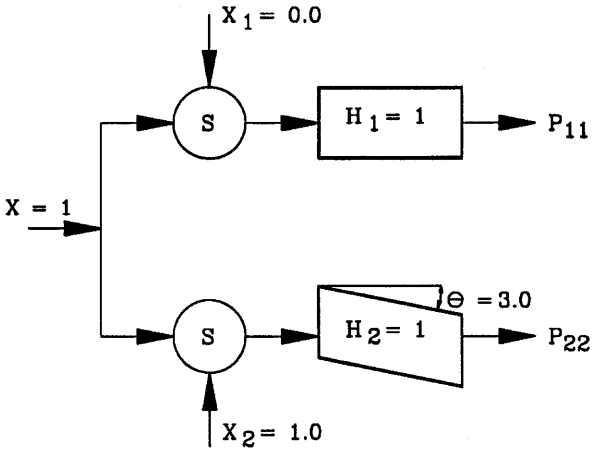

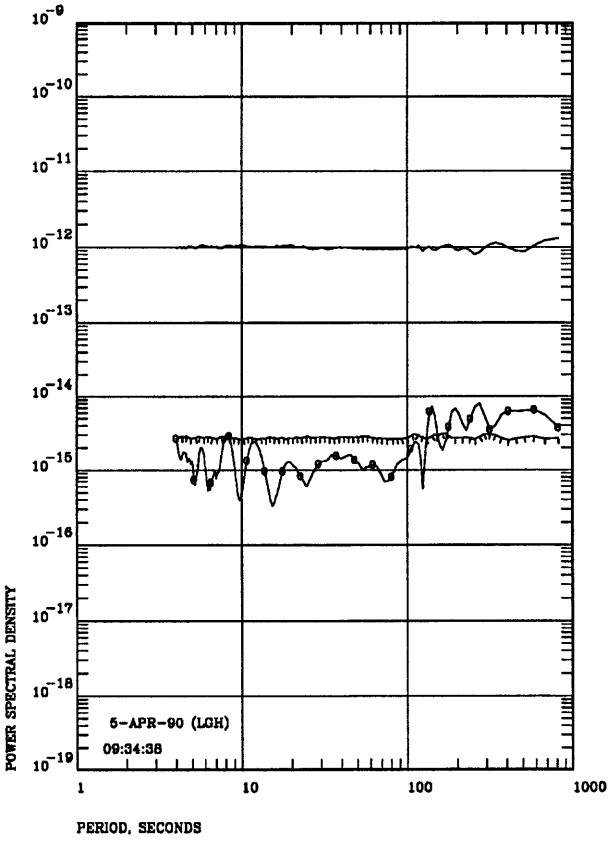

Figure 6.4 Linear system model and PSD estimates for a 3.0 degree misalignment of two sensors in a white noise environment. See Figure 4.1 for line definition.

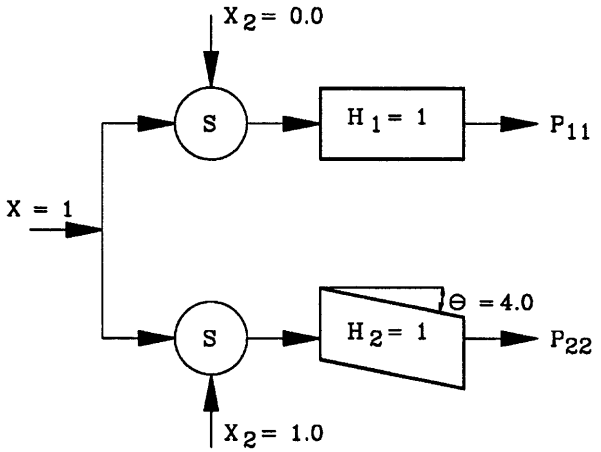

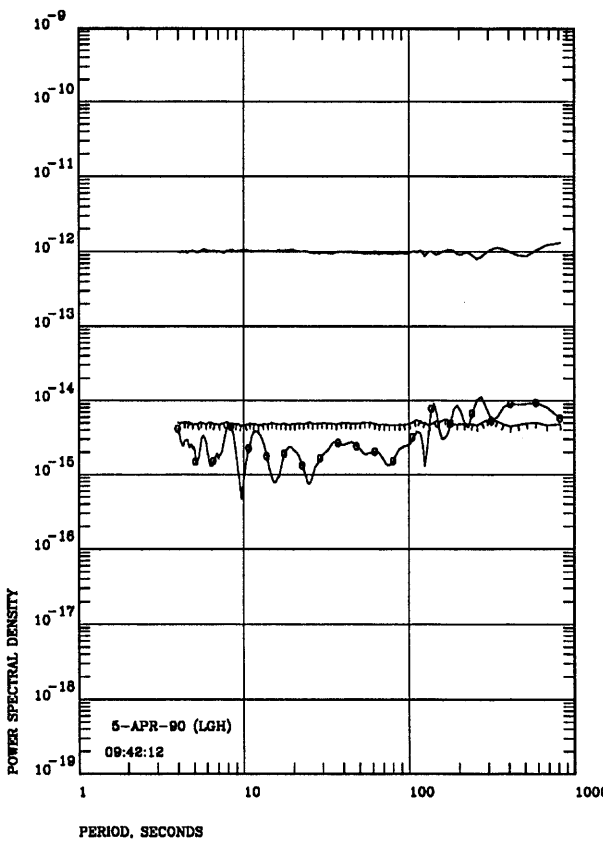

Figure 6.5 Linear system model and PSD estimates for a 4.0 degree misalignment of two sensors in a white noise environment. See Figure 4.1 for line definition.

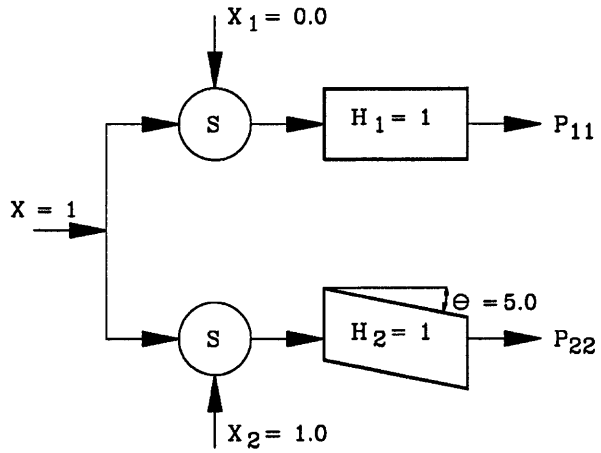

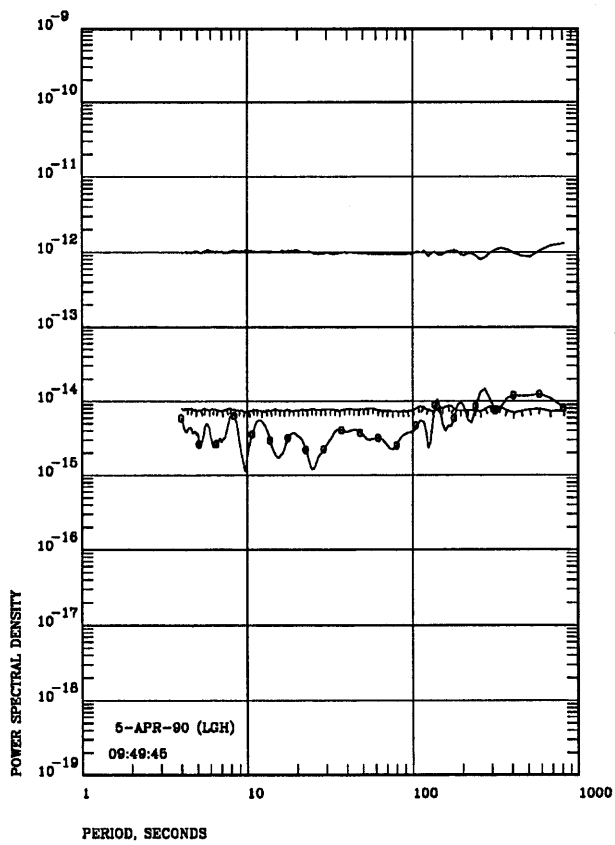

Figure 6.6 Linear system model and PSD estimates for a 5.0 degree misalignment of two sensors in a white noise environment. See Figure 4.1 for line definition.

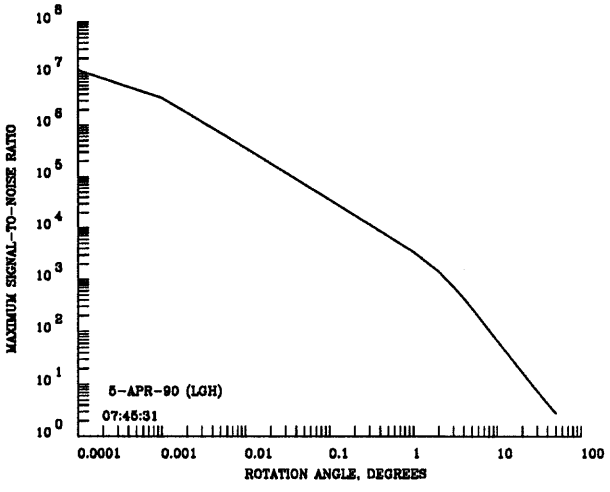

Figure 6.7 Maximum detectable SNR as a function of azimuthal misalignment on a log scale in a white noise environment.

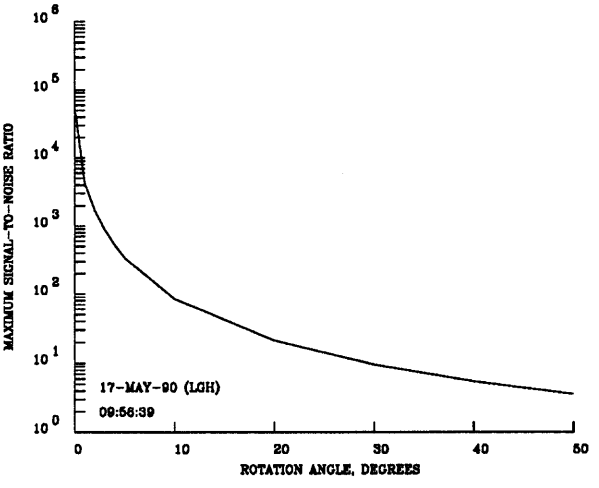

Figure 6.8 Maximum detectable SNR as a function of azimuthal misalignment on a linear scale in a white noise environment.

Since the PSD estimates of Figures 6.1 through 6.6 are rather rough, a better estimate of the true PSD level can be made by averaging the PSD over a band of the spectra. Averages of the resolution limits at all 14 of the misalignment angles listed above were calculated over the 4 to 100 second band using the following equation.

$$P_{ave} = \frac{1}{N}\sum_{i=1}^{N} P_i \qquad \textit{Equation} \quad 6.1$$

Here, N is the total number of PSD bins between 4 and 100 seconds (984), and P_i is the calculated PSD level in each bin.

These averages were then used to calculate the maximum SNR that can be resolved as a result of misalignment noise. The results are plotted as functions of the misalignment angle on log and linear scales in Figures 6.7 and 6.8. Note the rapid decrease in the maximum resolvable SNR with increase in the angle at small misalignments which is particularly evident in Figure 6.8. The same data over a more practical range of 0 to 5 degrees is presented in Figure 6.9. It is evident that one should not expect to be able to repeatedly resolve sensor noise levels with SNR's above approximately 1000 because reasonable alignment errors will mask noise levels below this figure.

The functional dependence of the coherence between the two sensors as a function of the misalignment angle is available as an interesting by-product of this analysis. The calculated coherence as a function of the misalignment angle is plotted in Figures 6.10 and 6.11 on log and linear scales respectively. In contrast to the strong dependence on the misalignment induced noise floor on angle at small angles in Figure 6.8, the coherence is not a strong function of the

angle at small angles. This is particularly evident over practical ranges of misalignment as shown in Figure 6.12. To enhance the resolution of the functional dependence of the coherence on misalignment, this data is replotted with an ordinate of $\log_{10}(1-\gamma^2)$ in Figure 6.13.

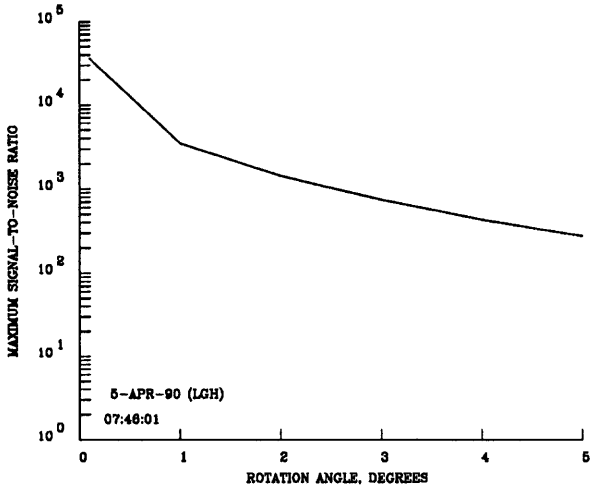

Figure 6.9 Maximum detectable SNR as a function of azimuthal misalignment over practical angles of misalignment.

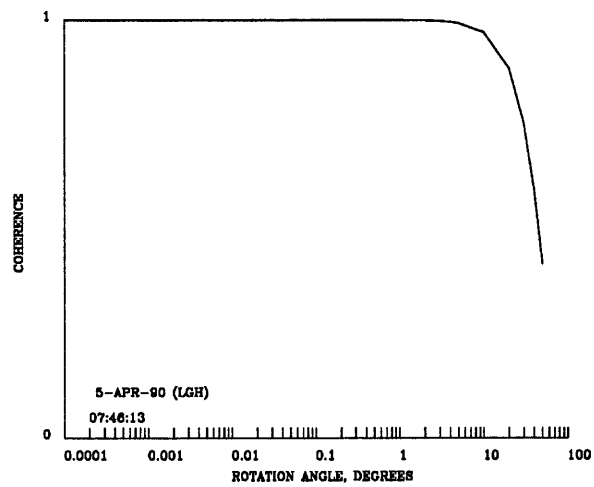

Figure 6.10 Coherence as a function of azimuthal misalignment on a log scale in a white noise environment.

Many have proposed that the coherence between a surface installed horizontal sensor and a borehole installed horizontal sensor be used as a method of determining the orientation of the borehole sensor. From Figure 6.13, it is evident that, in order to achieve reasonable accuracy in the orientation of the borehole instrument, quite high accuracies in estimating the coherence must be achieved. For instance, a resolution of the coherence to within one part in a hundred is necessary to achieve an orientation accuracy of approximately 5 to 6 degrees. This is difficult to do under field conditions with instrument separations of the order of 100 meters as would be encountered in a typical borehole installation.

The functional dependence of the coherence function on the angle of misalignment is illustrated in Figure 6.11 in which a plot of $\cos^2(\theta)$ is superimposed on the plot of the experimentally determined coherence data. The match in the two sets of data is so good that the $\cos^2(\theta)$ plot is barely discernable in the form of a slight thickening of the line at large misalignment angles. This result tends to confirm an unpublished derivation by Sorrells, 1981, in which he predicted that, in an isotropic noise field, the coherence should vary as $\cos^2(\theta)$.

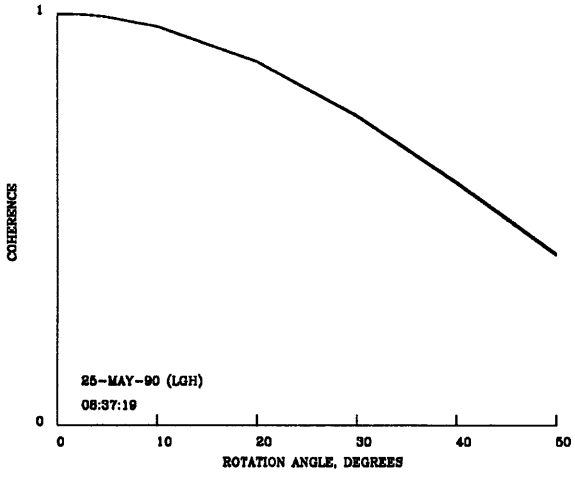

Figure 6.11 Coherence as a function of azimuthal misalignment on a linear scale in a white noise environment. A plot of $\cos^2(\theta)$ virtually overlies the plot of the experimentally determined data.

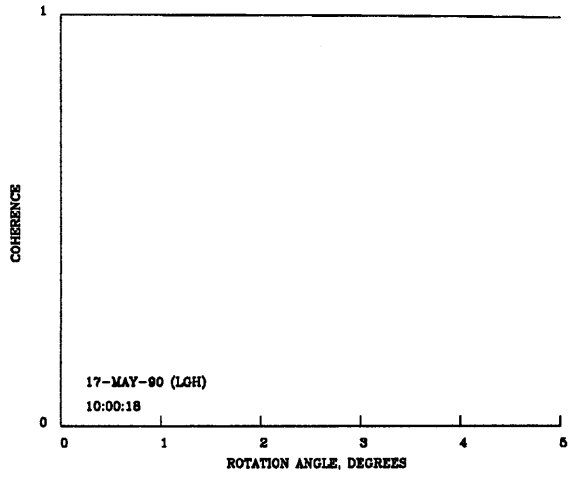

Figure 6.12 Coherence as a function of azimuthal misalignment over practical angles of misalignment.

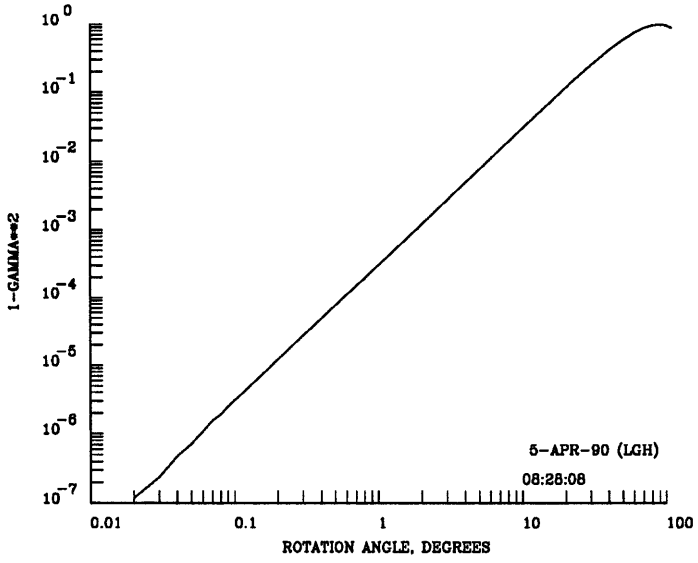

Figure 6.13 A plot of $1-\gamma^2$ as a function of azimuthal misalignment.

6.2 BANDSHAPED BACKGROUND

The effects of misalignment on the analysis of more realistic bandshaped earth background was simulated by generating two bandshaped orthogonal time series and adding them as depicted in the linear system model portions of Figures 6.14 through 6.19. The same Chebyshev type II bandstop filter as was described in Section 5.2 with a response as shown in Figure 5.7 was used to bandshape both incoherent white noise time series into a PSD spectra which resembles an earth background acceleration spectra. The filtered time series were then transformed and the input for channel 2 was rotated using Equation 6.1 to create a simulated misalignment for each set of data in Figures 6.14 through 6.19. The input to the first channel was assumed to be unrotated with $X_1 = 0$ as it was in Section 6.1. Data was processed for all 14 misalignment angles listed in Section 6.1, but only the results for the more practical misalignment angles are presented in detail in Figures 6.14 through 6.19.

In many respects, the results of this bandshaped background study resemble those of the white background misalignment study in the previous section. Figure 6.14 contains the results of the analysis of data which simulates a 0.1 degree misalignment; it can be compared with Figure 6.1 which contains the data for the same misalignment for a white background. The out of band misalignment generated PSD noise estimates in the two figures are approximately equal. The in band noise estimates of Figure 6.14 appear to maintain approximately the same relative level with respect to the input bandshaped background as do the corresponding estimated noise levels for the white background case in Figure 6.1. As the simulated misalignment angle increases, (see Figures 6.14 through 6.19) the estimated noise levels increase as they did in the white noise case. Once again, the ability of the model to resolve real sensor noise is limited by misalignment generated noise.

An important observation to make is that the misaligned bandshaped background generated noise spectral shapes follow the background spectral shape in all cases. This was also true of the previous white noise examples but the effect was not nearly as dramatic. Furthermore, note once more that the noise estimates calculated in Section 5.2, which simulated a white instrument noise buried in a bandshaped earth background spectra, did not follow the background spectral shape. A combined study of these two sets of data leads one to conclude that the spectral shape of the calculated noise data in this section and the spectral shape of most real world noise test data must be heavily influenced by misalignment generated noise contamination. The spectral shape of the calculated noise estimates does not appear to be due to numerical precision problems because the noise estimates of Section 6.1 are white. Instead, the results of Sections 6.1 and 6.2 indicate that the shape of real world noise estimates appears to be entirely due to the fact that it is impossible to repeatedly align two sensors perfectly.

True instrument noise may be completely buried in misalignment noise in certain parts of the spectrum if very careful measures are not followed to align the sensors quite precisely. This is especially true in the shorter period regions of the long period band (2 through approximately 20 seconds) in which the calculated sensor noise spectra from actual test data almost always duplicate the spectral shape of the observed earth background; the calculated noise spectra is merely shifted down in PSD level by a more or less constant factor throughout this period range. Since true instrument noise spectra should not necessarily be expected to duplicate earth background spectra, the hypothetical instrument noise levels normally calculated from real test data throughout this spectral range are probably composed entirely of misalignment generated noise!

This does not mean that misaligned test data is invalid; it means that it must be interpreted properly. Based on the results seen here, the proper interpretation is to assert that the true sensor noise must lie at or below the levels calculated from the model. The analysis merely places an upper limit on the actual sensor noise. True sensor noise may be considerably less than the analysis process indicates depending on the degree of misalignment.

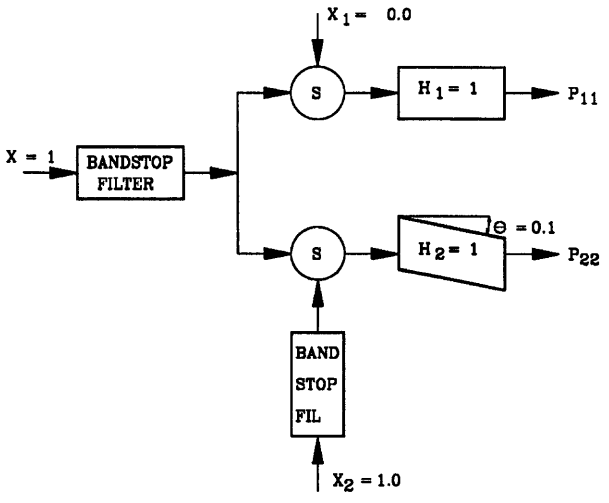

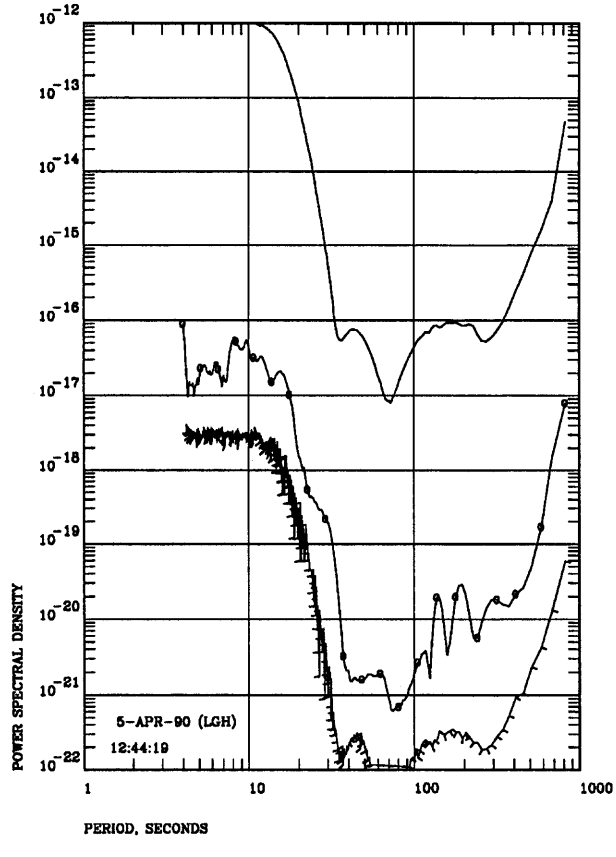

Figure 6.14 Linear system model and PSD estimates for a 0.1 degree misalignment of two sensors in a bandshaped noise environment. See Figure 4.1 for line definition.

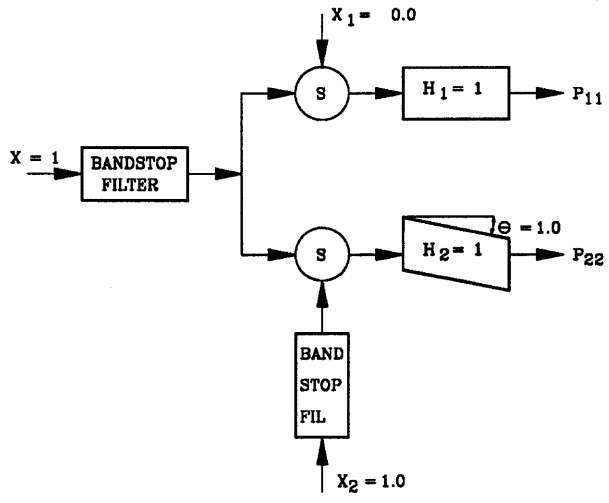

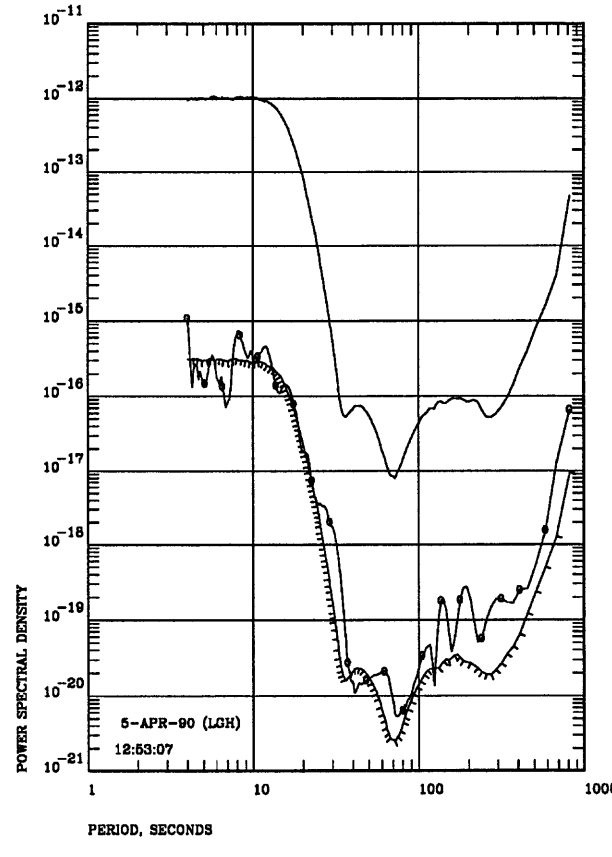

Figure 6.15 Linear system model and PSD estimates for a 1.0 degree misalignment of two sensors in a bandshaped noise environment. See Figure 4.1 for line definition.

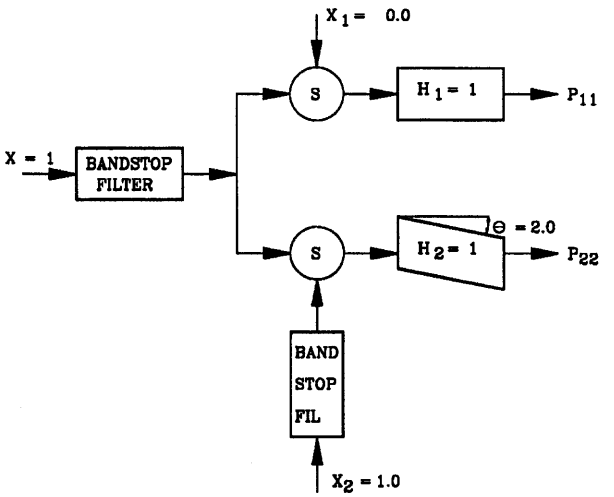

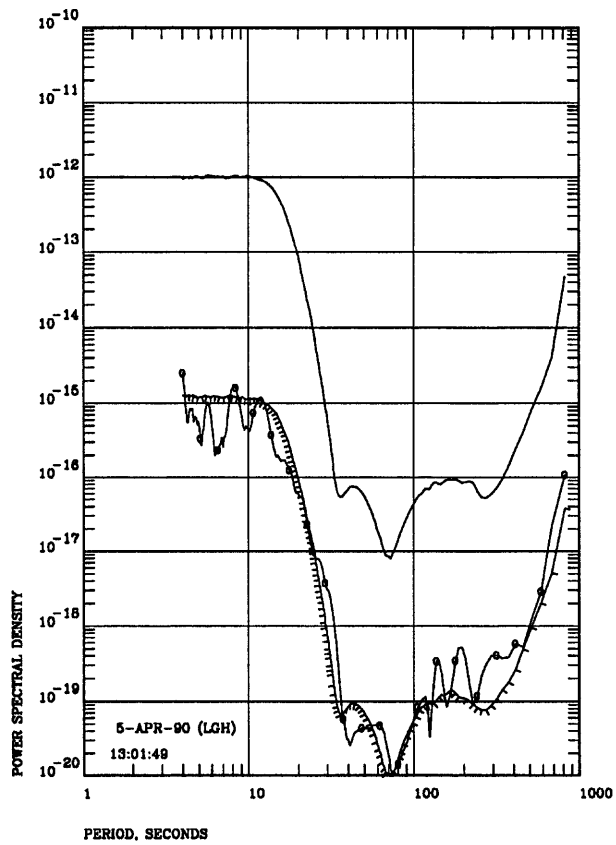

Figure 6.16 Linear system model and PSD estimates for a 2.0 degree misalignment of two sensors in a bandshaped noise environment. See Figure 4.1 for line definition.

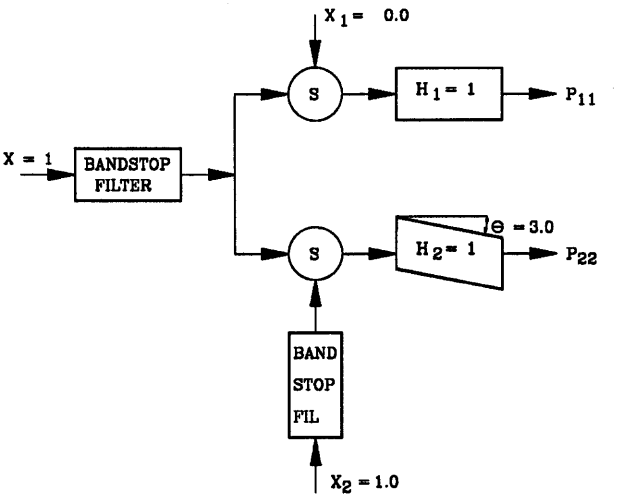

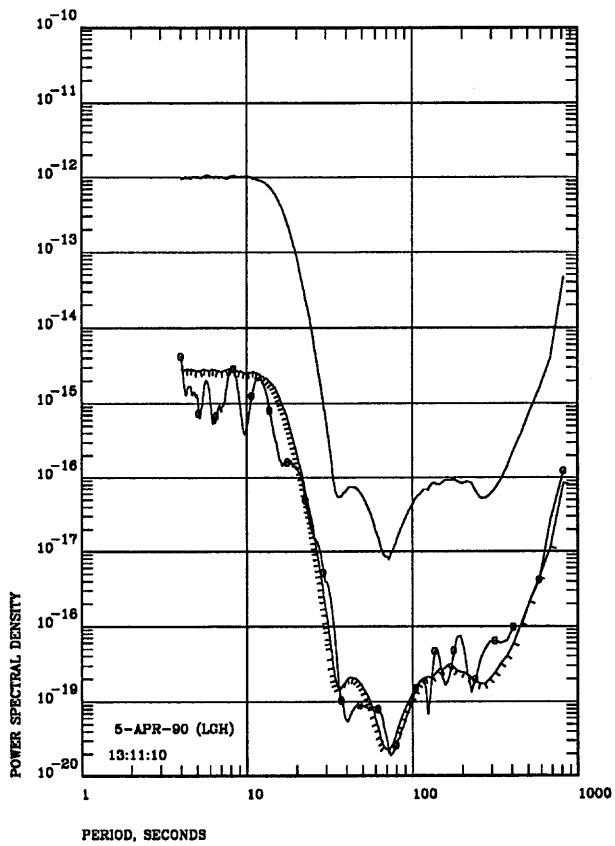

Figure 6.17 Linear system model and PSD estimates for a 3.0 degree misalignment of two sensors in a bandshaped noise environment. See Figure 4.1 for line definition.

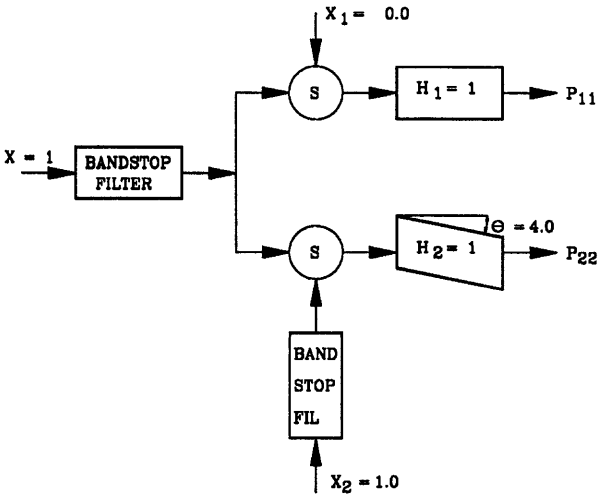

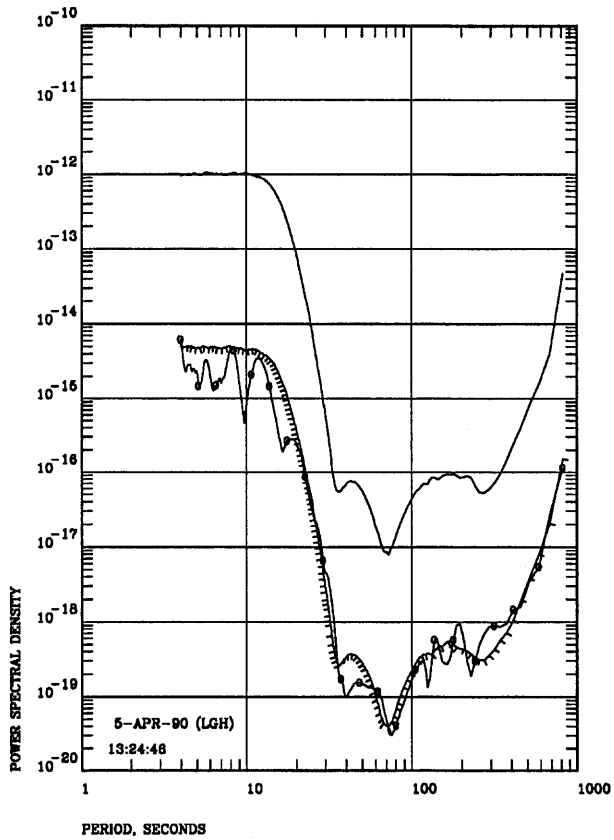

Figure 6.18 Linear system model and PSD estimates for a 4.0 degree misalignment of two sensors in a bandshaped noise environment. See Figure 4.1 for line definition.

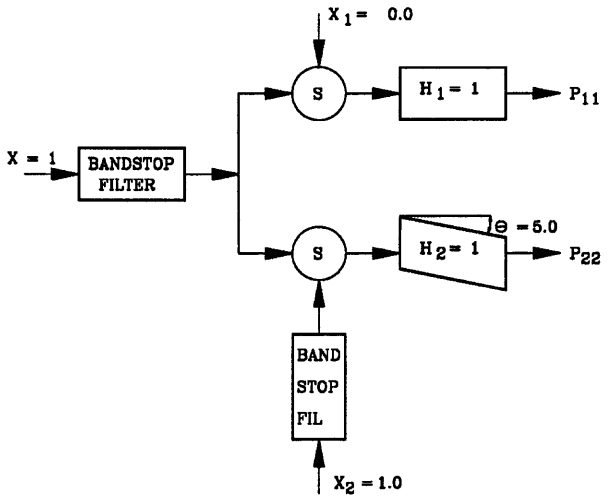

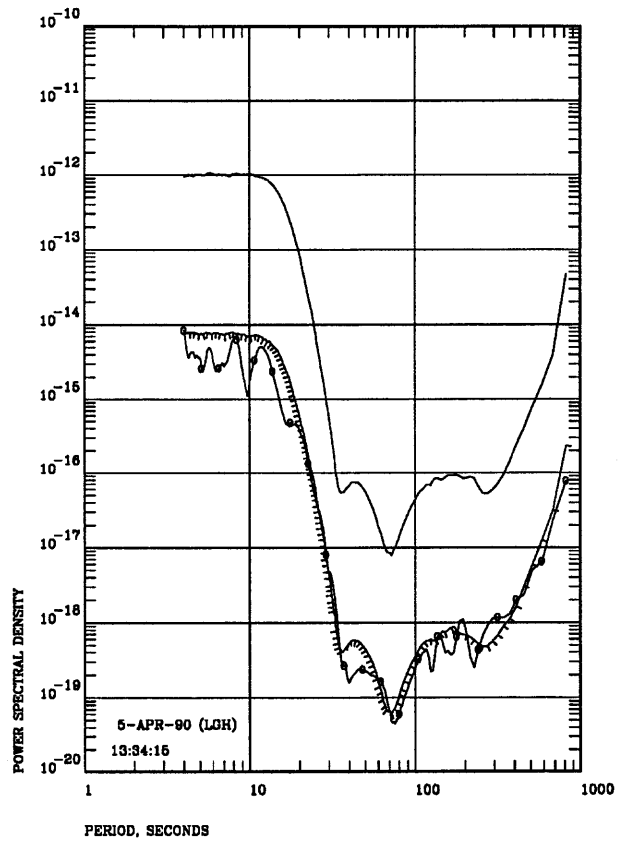

Figure 6.19 Linear system model and PSD estimates for a 5.0 degree misalignment of two sensors in a bandshaped noise environment. See Figure 4.1 for line definition.

At first glance, it may seem that the gap between the total noise power (P_{11}) and the calculated noise power (N_1 in Figures 6.14 through 6.19) narrows in the region between 10 and 30 seconds. This is an illusion which is due to the fact that the PSD curves are quite steep in that part of the spectrum. The ratio of the total noise power to the calculated noise power is essentially a constant as a function of period as the following analysis demonstrates.

The averaging technique used in Section 6.1 (see Equation 6.1) to calculate maximum detectable SNR's cannot be directly applied to the bandshaped data of this section because averaging from 4 to 100 seconds would smooth out much of the bandshaping. However, averaging over narrower bands should yield reasonable estimates of the maximum detectable SNR within those bands. Maximum detectable SNR's were calculated in narrow subbands centered about 6, 10, 20, 40, 100, and 500 seconds using the expression

$$P_{ave} = \frac{1}{N} \sum_{i=1}^{N} P_{j-\frac{N}{2}+i} \qquad \textit{Equation} \quad 6.1$$

where P_{ave} is the average PSD within the selected band, N is the total number of points averaged, j is the bin index of the center bin over which the average is calculated, and i is the bin index running the width of the subband being averaged.

SUB-BAND (SECONDS)	NUMBER AVERAGED (N)	CENTER BIN INDEX (j)
6	60	343
10	60	616
20	30	821
40	30	923
100	30	984
500	16	1016

Table 6.1 Definition of subbands for averaging PSD's to calculate maximum SNR's.

Table 6.1 summarizes the parameters which define the subbands over which the data was averaged and Figure 6.20 contains the maximum SNR estimates obtained by summing over all six subbands. No effort has been made in Figure 6.20 to identify which curve belongs to which subband because all curves are quite similar. Note that the six curves are very similar to the results obtained for the white background misalignment data in Section 6.1 (Figure 6.7). The indication is that the bandshaped noise PSD data has the same shape as the bandshaped background PSD data. The whole PSD curve is just shifted down in PSD by an amount which is a function of the misalignment angle.

If this is true, then the maximum SNR's calculated for the six subbands for a given misalignment angle should all be equal. The six SNR's for six misalignment angles are plotted as functions of the period in Figure 6.21. Indeed, these plots approximate horizontal straight lines as they should if the noise PSD retains the shape of the bandshaped background PSD.

The reason that both the direct method and the asymptotic maximum method produce misalignment noise is because the linear system model of Figure 2.1 which was used to derive the system equations is invalid. That model assumes that the ground input to both sensor systems (X) is coherent. This is not the case if the sensors are not aligned. A more sophisticated model could adequately describe misaligned sensors but to do so would require the knowledge of the unknown misalignment angle.

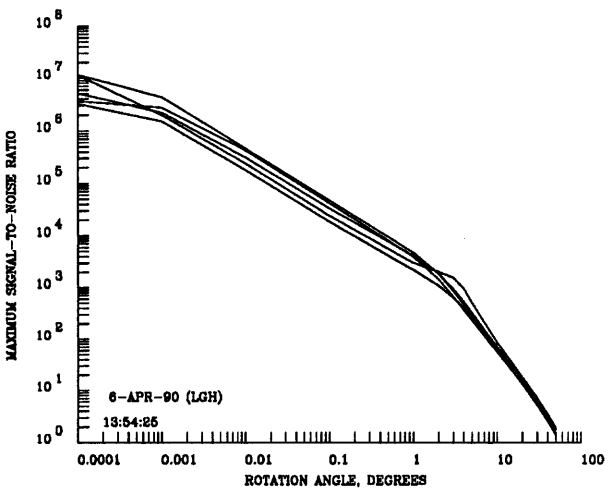

Figure 6.20 Maximum detectable SNR as a function of azimuthal misalignment on a log scale in a bandshaped background. Curves are from data centered around 6, 10, 20, 40, 100, and 500 seconds.

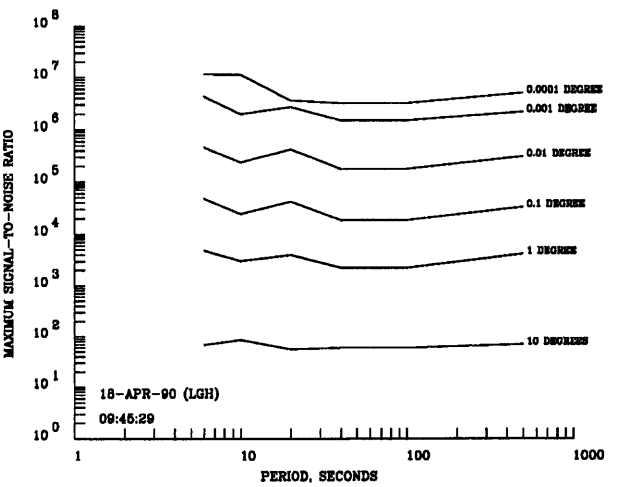

Figure 6.21 Maximum detectable SNR as a function of period for several values of constant azimuthal misalignment.

Finally, the functional dependence of the coherence function on the angle of misalignment in a bandshaped earth background is shown in Figure 6.22. The coherence data was obtained by averaging the coherence across the six second band defined in Table 6.1. The agreement with the $\cos^2(\theta)$ curve superimposed on the plot is not quite as good as in the white background case shown in Figure 6.11, but it is still an excellent fit.

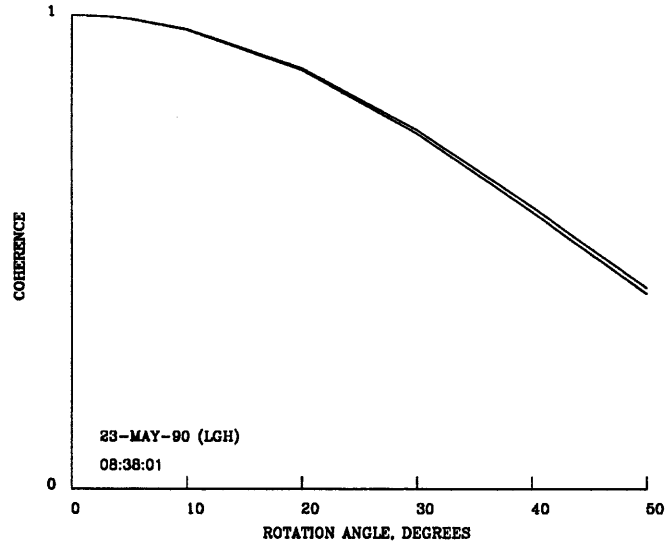

Figure 6.22 Coherence as a function of azimuthal misalignment on a linear scale in a band-shaped noise environment. A plot of $\cos^2(\theta)$ is superimposed on the experimentally determined data.

7 QUIET SITE VERSES NOISY SITE TESTING

The results presented above constitute strong evidence that comparative seismometer test and evaluation studies, which are aimed at establishing the actual noise levels in modern quiet sensors, should be carried out at quiet sites. The argument is as follows. For a given fixed alignment error, the lower the site earth background levels, the lower will be the misalignment error induced levels of model calculated noise in absolute terms. This means that lower levels of real instrument noise can be resolved at quiet sites for a given alignment error. If the site is too noisy, misalignment generated noise levels will rise above the true instrument noise thereby masking the true instrument capability. Note that the site need be quiet only in the band of interest for the tests. High levels of out of band earth background should not interfere with the measurements; at least high levels of out of band background will not cause high levels of in band misalignment noise.

8 HIGH BACKGROUND LINEARITY MEASUREMENTS

The results of this study also indicate that the interpretation of changes in the calculated noise levels of an instrument under low and high background as being indicative of the degree of linearity are probably not valid. Even a pair of perfectly linear but misaligned instruments will produce a change in the calculated noise levels between low and high background conditions if any of the change in background level occurs within the band in which linearity induced PSD level changes are sought.

9 CONCLUSIONS AND RECOMMENDATIONS

This study has investigated the effects of several potential sources of error in the analysis of the data obtained from side-by-side testing of seismic sensors. Errors arising from the mathematical processing of the data do not appear to be too serious at realistic levels of SNR likely to be found in real world sensors. However, errors in estimating noise levels arising from the physical misalignment of the two sensors under test do appear to be potentially serious. It is highly probable that most noise spectra obtained to date are contaminated with noise power resulting from a misalignment problem.

The author recommends that comparative seismometer evaluation studies be conducted at quiet sites to minimize misalignment contamination of test data.

Comparative noise levels derived under low and high background conditions should not be attributed entirely to linearity problems in the instrument.

The author recommends that advanced methods of precisely aligning sensors be developed and put into standard use in sensor test procedures.

As a final note, the author *suspects* that it may be possible to correct for unknown alignment errors by using more than two sensors to conduct the tests and a more complex mathematical model to process the data. This topic *may* be the subject of a subsequent report.

10 REFERENCES

Bath, Markus, (1974), "Spectral Analysis in Geophysics" Elsevier Scientific Publishing Company, Amsterdam - Oxford - New York

Bendat, Julius S., Piersol, Allan G., (1971), "Random Data: Analysis and Measurement Procedures" *John Wiley & Sons, Inc.*

Holcomb, L. Gary, (1989), "A Direct Method for Calculating Instrument Noise Levels in Side-by-Side Seismometer Evaluations" *U.S. Geological Survey Open-File Report 89-214, 35 p.*

Peterson, J., Hutt, Charles R., Holcomb, L. Gary, (1980). "Test and Calibration of the Seismic Research Observatory" *U.S. Geological Survey Open-File Report 80-187, 86 p.*

Stearns, Samuel D., (1975), "Digital Signal Analysis" *Hayden Book company, Inc., Rochelle Park, New Jersey*

Stearns, Samuel D., David, Ruth A. (1988). "Signal Processing Algorithms" *Prentice-Hall, Inc., Englewood Cliffs, New Jersey*

Sorrells, G. G., (1981), Unpublished (Courtesy of Jim Durham, Sandia National Laboratories)